California Institute of Technology

SURF 2005

Final Report

Performance Improvement of the Geometric Anti Spring (GAS) Seismic Filter for Gravitational Waves Detectors

Student

Alberto Stochino
University of Pisa, IT

Mentor

Riccardo DeSalvo
LIGO Project

LIGO-T0500239-00-D

Abstract

Seismic noise is the most relevant source of low frequency disturbances for gravitational waves interferometric detectors. The displacement of the mirrors due to the ground motion changes the length of the arm limiting the sensibility to actual incoming signals. The ground motion amplitude is of the order of 10^{-6} m, the expected gravitational wave signal is less than 10^{-18} m, consequently the required attenuation factor is of at least 10^{-12}. In first approximation the vertical motion of the mirrors is orthogonal to the interferometer beam plane and does not affect the interferometric measurement. Coupling between the degrees of freedom is minimized, but, in practice, vertical noise is reinjected in the horizontal plane at each filtering stage at the percent level. Therefore vertical seismic attenuation at the level of 10^{-10} is required. The Geometric Anti-Spring Filter (GAS) was developed to achieve this aim. The filter performs very well above 10 Hz giving an attenuation of 60 dB. Until this work each filter could not provide more than 60 dB because of the high frequency saturation typical of all passive mechanical filters. Virgo, the first experiment, using (magnetic) anti spring filters, was limited to 40 dB per filter and required attenuation towers with 6 filters. Better filter performance will allow the construction of shorter, cheaper and easier to handle attenuation chains.

The subject of this thesis is the improvement of the attenuation performance of vertical oscillators. We studied, designed and built a device, based on the principle of compensation of the center of percussion effect, to be mounted in parallel to the blade springs of the GAS filters.

The performance attenuation of the GAS filters is limited by the momentum of inertia of its blades, which couple-in a fraction of the seismic excitation through the process called Center Of Percussion effect. Until presently this limitation was deemed unavoidable because of the flexibility of the blade that precludes the installation of a suitable blade counterweight. The device that we invented is basically a wand with

counterweights to generate a negative center of percussion effect optimally tuned to externally compensate that of the blade springs. The wand was designed taking inspiration from the counterweights implemented, for the same reason, on the inverted pendula used for horizontal attenuation. We built and installed a prototype, made of carbon fiber for lightness, and measured its performance as a function of counterweight tuning. Measuring the transfer function we observed the system working as expected. The device could compensate, under- and overcompensate the COP effect. When overcompensating, we observed the expected notch appearing at the high frequency end of the $1/f^2$ filter attenuation slope, followed by a saturation level different from the original one. By tuning the position of the counterweight we could move this notch up and down in frequency and succeeded in making it disappear at high frequency. When this was done the saturation limit was measured to be 80 dB, which is one order of magnitude improvement in the previous attenuation performance. Even better attenuation performances may be possible with finer counterweight tuning, impossible in our rather primitive testing setup.

The device improving the GAS filter performance will be immediately implemented in the HAM SAS optic table seismic attenuators. These improved GAS filters will also be implemented in the LCGT interferometer and, likely, in other mirror suspension chains of future interferometers.

This work was performed over 12 weeks during the summer 2005 at the LIGO SAS Laboratories of California Institute of Technologies in Pasadena.

This material is based upon work supported by the National Science Foundation under Grant No. PHY-0107417.

Contents

Chapter 1

GRAVITATIONAL WAVES DETECTION

1.1 Gravitational Waves

Gravitational Waves (GWs) are perturbation of spacetime, which propagates at the speed of light. They were predicted by Einstein as one of the consequences of the theory of General Relativity in 1916. Their existence has been only indirectly proven by the observation of the decay of the orbital period binary pulsar PSR1913+16 by Taylor and Hulse and other three similar pulsar systems. Direct detection of the GW has been attempted as the validation of the theory of General Relativity.

The detection of GWs is one of the frontiers in the modern astronomy, it is expected to open a new window for astronomical observations. As the interaction between the GW and matter is so small, detectable GWs are expected to be generated only by dynamical and relativistic acceleration of massive stars, one of the most interesting subjects in astronomy.

1.2 Interferometric Detection of Gravitational Waves

A Michelson interferometer is an optical configuration used to detect the phase difference accumulated in different optical paths. It is applied in various fields as metrology and solid state physics. Laser interferometric GW detection is a very direct application of this optical system. The mirrors that form a Michelson interferometer for GW detection must be allowed to follow the distorted spacetime: i.e. the mirrors must "float" in an inertial frame. In practice this fundamental requirement is achieved in the horizontal plane by suspending each optical component of the interferometer from a pendulum. The fraction of the GW-induced distortion projected on the horizontal plane becomes detectable.

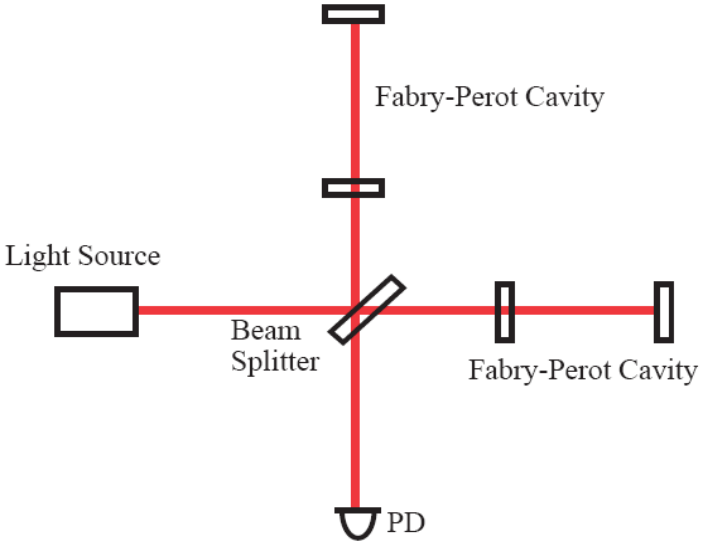

A Michelson interferometer scheme

The laser beam is split at the surface of the beam splitter (BS) into two orthogonal directions. At the end of each arm a suspended mirror reflects the beam back to the BS. The beams reflected from the arms recombine on the BS surface. A fraction of the recombined beam transmits through the BS and the rest is reflected from it. The intensity of each recombined beam is determined by the interferometer conditions and is detected by a photo detector (PD) that gives the differential position signal from the apparatus.

Gravitational Waves can be detected by measuring their tidal action on a distribution of “free–falling” masses. The two end mirrors of a Michelson interferometer can be used for this purpose. When the mirrors in the interferometer move along the optical axes around their nominal position, they cause a phase shift detectable by the interferometer.

The optimal solution would be to build M. interferometers with arms as long as ½ of the GW wavelength, which would require hundreds or thousands of km. Since the arm length is limited by the Earth curvature (and by budget reasons) to a few Km, folding the light path into an optical cavity (Fabry–Perot) is necessary. A Fabry-Perot Michelson Interferometer is a Michelson Interferometer instrumented with a Fabry-Perot cavity instead of a single mirror in each arm.

1.3 The GW Detectors: Virgo and LIGO

Based on this idea several interferometric antennas are being built in the world: a 3–Km detector in Italy (VIRGO), a 600–m in Germany (GEO600), a 300–m in Japan (TAMA) and two twin 4–Km and a 2–Km in USA (LIGO).

The LIGO project is a National Science Foundation sponsored project managed jointly by the California Institute of Technology and the Massachusetts Institute of Technology. The project comprehends two large interferometer observatories, one in eastern Washington state on the U.S. Department of Energy's Hanford Site and the other in Livingston, Louisiana. Two widely separated sites are required so that environmental perturbations to the interferometers can be expected to be independent and hence uncorrelated. The GW signals will be correlated and this property is used in making the observation.

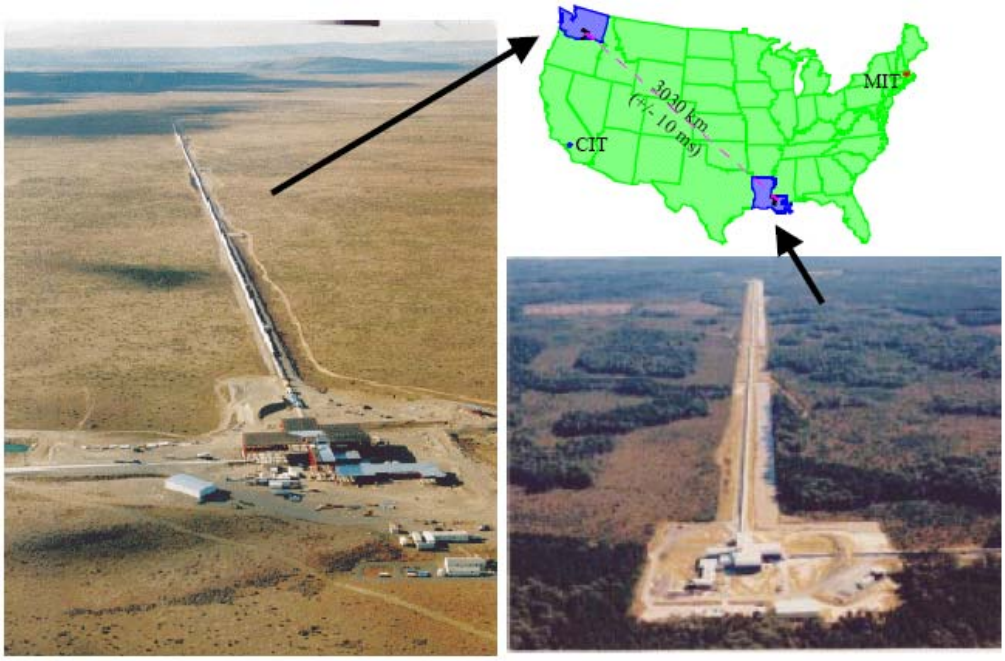

LIGO Observatories: Hanford, Washington and Livingston, Louisiana

Virgo is located within the site of EGO, European Gravitational Observatory, based at Cascina, near Pisa on the river Arno plain.

The frequency range of Virgo extends from 10 to 6,000 Hz. This range as well as the very high sensitivity should allow detection of gravitational radiation produced by

supernovae and coalescence of binary systems in the milky way and in outer galaxies, for instance from the Virgo cluster.

The Virgo interferometer, Cascina (Pisa), Italy

Virgo has been funded by the French CNRS (Centre National de la Recherche Scientifique) and the Italian INFN (Istituto Nazionale di Fisica Nucleare). Virgo is the result of a close collaboration between several hundreds of French and Italian physicists and engineers belonging to eleven research laboratories.

1.4 Sources of Noise

Measuring length deviations smaller than the proton radius puts high requirements on the technology used to build these instruments. It also requires a good understanding of physical and technical noise sources which may limit the gravitational wave sensitivity. The design sensitivity of the Laser Interferometer gravitational wave Observatory (LIGO) Project is shown in the next figure. It shows that the sensitivity at low frequency, $f < 50$ Hz, is due to seismic noise, at intermediate frequencies, $50 \text{ Hz} < f < 150$ Hz, due to thermal noise and at high frequencies, $f > 150$ Hz, due to laser shot noise.

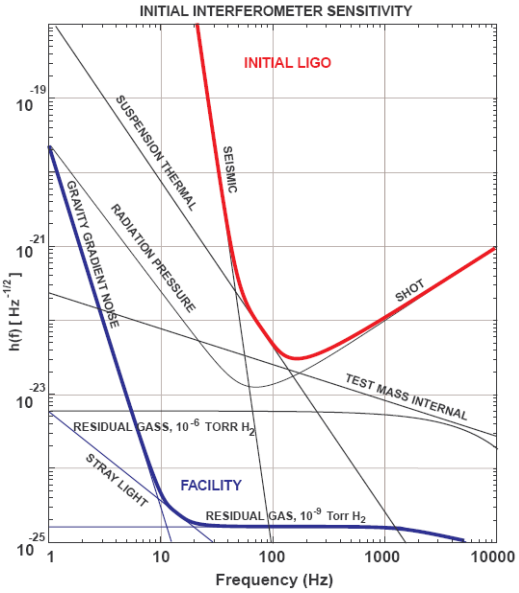

Design sensitivity for LIGO

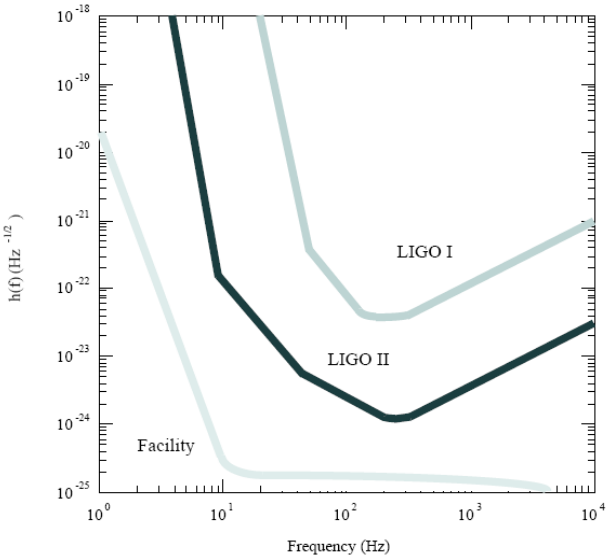

Sensitivity improvements expected for LIGO II.

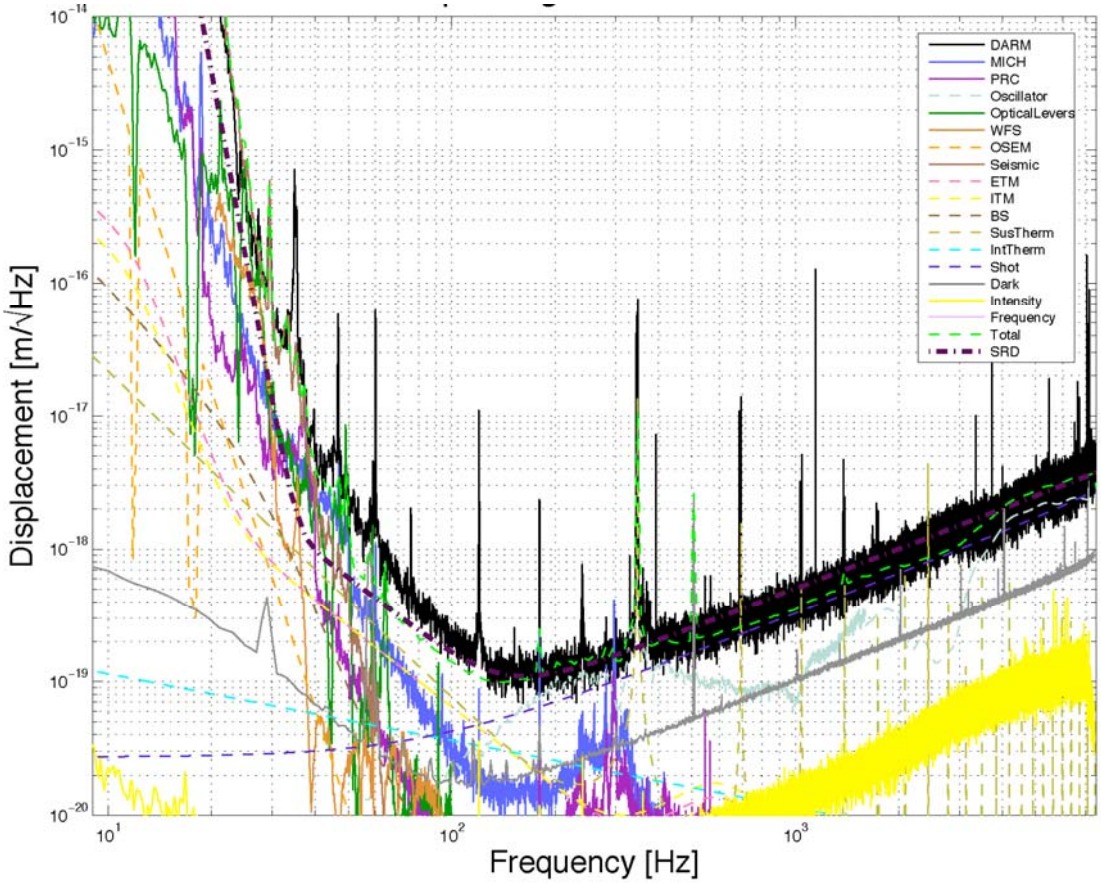

The LIGO sensitivity latest data shows the seismic noise being dominant at low frequency

Chapter II

SEISMIC ATTENUATION

2.1 Seismic noise

Seismic motion is an inevitable noise source for interferometers built on the Earth's crust. The signal of an interferometer caused by the continuous and random ground motion is called seismic noise. The ground motion transmitted through the mechanical connection between the ground and the test masses results in perturbations of the test masses separation. Seismic motion is excited by the natural phenomena like macro-seismic events, thermal and tidal stress upconversions, oceanic, and atmospheric activities, as well as by the human activities.

Since the ground motion is of the order of 10^{-6} m and the expected GW signal is less than 10^{-18} m, we need attenuation factors of the order of 10^{-12}.

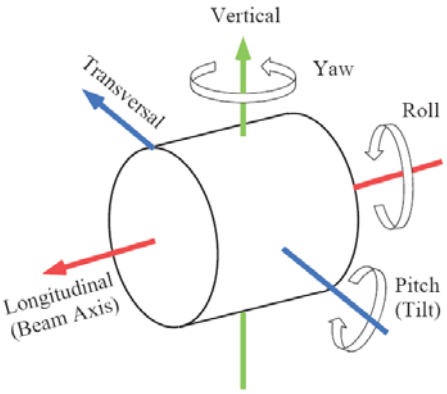

Payload degrees of freedom

The required seismic attenuation is obtained using a chain of mechanical oscillators of resonant frequency lower than the frequency region of interest. In the horizontal

direction the simple pendulum is the most straightforward and effective solution: the suspension wire has a negligible mass and the attenuation factor behaves like $1/f^2$ till the first violin mode of the wire (tens or hundreds of Hertz). Thus, with reasonable pendulum lengths (tens of cm), good attenuation factors can be easily achieved in the frequency band of interest for the x y and normal modes. A simple pendulum is even more effective for the yaw (Φ) mode; torsional frequencies of few tens of millihertz are easy to be obtained. A mass suspended by a wire has also two independent degrees of freedom of tilt, the pitch (θ_x) and the roll (θ_y); low resonant frequencies (<0.5 Hz) and high attenuation factors for these modes are obtained by attaching the wire as close as possible to the center of mass of the individual filters.

The difficult part in achieving high isolation in all the 6 d.o.f.s is to generate good vertical attenuation. The vertical noise is, in principle, orthogonal to the sensitivity of the interferometer. Actually the 0.1–1% of the vertical motion is transferred to the horizontal direction at each attenuation stage by mechanical imperfections, misalignments and, ultimately (at the 10^{-4} level), by the non parallelism of verticality (the Earth curvature effects) on locations kilometers apart. The vertical attenuation then becomes practically as important as the others.

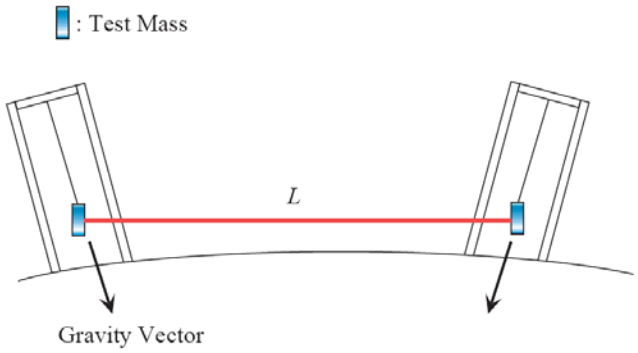

Vertical to horizontal coupling of the mirror motion caused by misalignment of gravity vector

2.2 Passive Mechanical Filters

Passive mechanical filtering is realized using the elasticity of mechanics. The simplest example is the ball suspended by a spring:

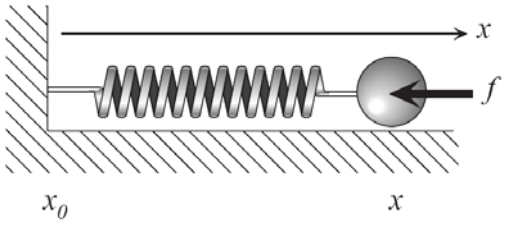

Simple example of passive mechanical filter

Assuming that the ball can move only along the x axis, its equation of motion in the frequency domain is

$$-m\omega^2 x - M\omega^2 x_0 = -k(1+i\phi)(x-x_0) - i\gamma\omega x$$

Here x and x_0 are the position of the ball and of the suspension point. m, is the mass of the ball, while M is the parameter determined by the mass distribution in the spring, k is the stiffness of the spring. γ and ϕ represents the coefficient of the damping due to the viscosity of medium around the ball and the internal energy dissipation due to the spring. From the above equation, the motion of the ball is related to the motion of the suspension point as

$$x = H_x(\omega)x_0$$

where H_x, the motion transfer function from the suspension point, is

$$H_x(\omega) \equiv \frac{\omega_0^2(1+i\phi) + \frac{M}{m}\omega^2}{\omega_0^2(1+i\phi) - \omega^2 + i\frac{\gamma}{m}\omega}$$

$\omega_0 = k/m$ being the angular resonant frequency of the system.

The plot of the TF shows the characteristic behaviour of passive mechanical filters in the approximation that the viscous damping iγωx is negligible:

- The motion of the ball is equal to that of the suspension point at low frequencies ($\omega << \omega_0$)
- The motion of the ball increases around the resonant frequency ω_0 and the phase rotates by -90 degrees at the resonant frequency, and -180 degrees above it.
- Above the critical frequency represented by $\omega_c = \sqrt{m/M}\,\omega_0$, the magnitude of the transfer function saturates at the level of M/m.

- Between the resonant frequency and the critical frequency, the amplitude of the transfer function reduces proportionally to $1/\omega^2$. This corresponds to the suppressed transmission of the ground motion to the suspended object.

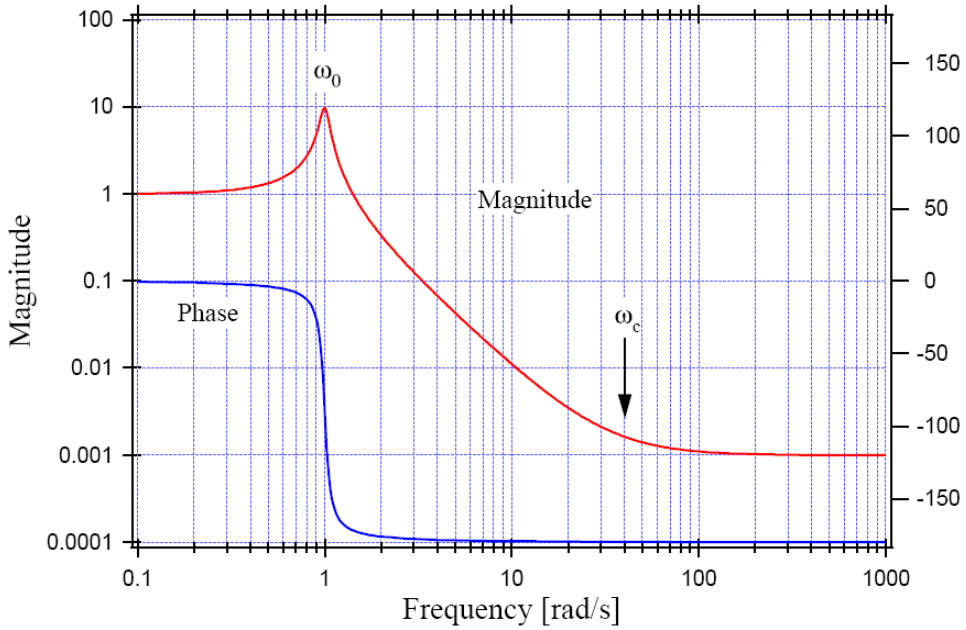

Standard transfer function of passive mechanical filters

2.3 Monolithic Geometric Anti-Spring Filter (MGASF)

Cross-coupling between vertical and horizontal (longitudinal) modes potentially limits the performance of mechanical isolation systems. Thence the vertical isolation must be designed at least not to be the limiting factor of the overall performance. Geometric Anti-Spring (GAS) is the solution developed for SAS, and it realizes low frequency resonance, typically about a few hundreds of mHz, based on linear anti-spring effect.

The GAS is a set of radially arranged cantilever springs, mounted from a common retainer ring structure and opposing each other via a central disk. The payload to be isolated is connected to the central part. The blades are completely flat when manufactured and flex like a fishing rod under load. They are mounted on clamping devices with an appropriated initial angle to accommodate the bending. The clamping devices are positioned to introduce a suitable radial and horizontal compression of the blades.

View of the MGAS blades mounted on the retainer ring

The radial stress tends to release itself by pushing the system up or down, thus generating a negative spring constant. In other words, the constrained geometry produces a non–linear force vs. displacement behavior with a flat region ($\partial F_z/\partial z \leq 0$) around the point of operation. The radial compression depends only on the geometry, particularly on the central disk diameter and on the distance between the clamping points of the blades. The geometric anti–spring (GAS) effect can then be tuned and, in principle, an arbitrarily low vertical resonant frequency can be achieved.

The GAS works as a normal harmonic oscillator in the vertical direction along which has transfer function

$$H_z(\omega) = \frac{\omega_0^2}{\omega_0^2 - \omega^2}$$

where $\omega_0^2 = k_{eff} / m$ is the local angular frequency of the vertical resonance.

Looking at the transfer function for a MGAS filter we can recognize the typical behavior of the harmonic oscillator at frequencies lower than a critical value (about 7-8 Hz). The plot shows the resonance peak about 0.2 Hz then the trend inversely proportional to the square of the frequency. Above the critical frequency the system does not follow anymore the harmonic slope towards zero and stops at a certain level where it saturates. The difference is attributed to the distributed mass of the springs, which introduces an inertial behavior in the response. Thence a realistic transfer function will be:

$$H_z(\omega) = \frac{\omega_0^2 - \beta\omega^2}{\omega_0^2 - \omega^2}$$

where β should be a function of the mass distribution in the blades and of the payload mass.

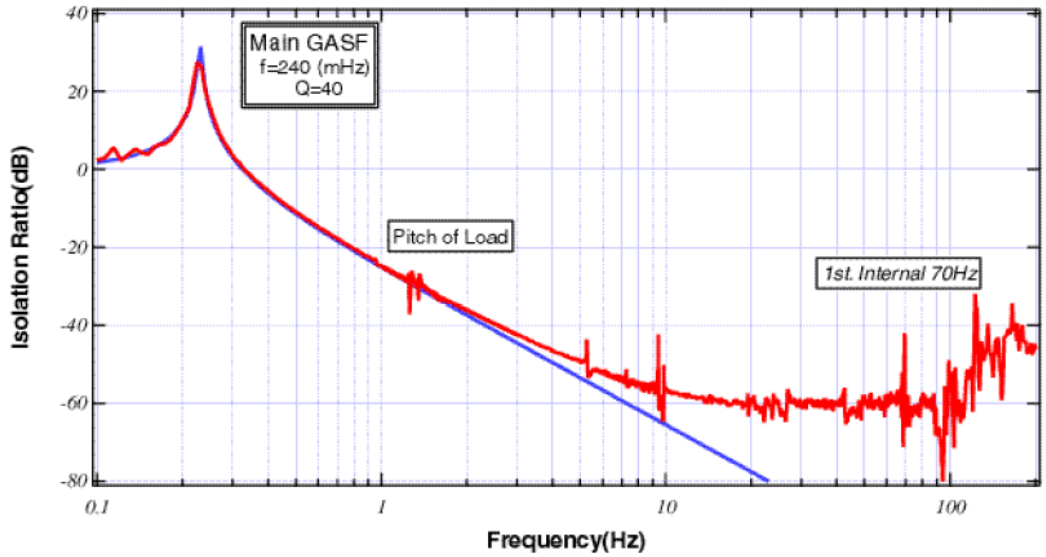

Attenuation properties of a MGAS filter with 2 mm thick blade. The attenuation behaves like $1/f^2$ from the main GASF resonance to a plateau of 60 dB. The structures about 1 Hz are simply payload pitch modes. Both measurements are dominated by acoustic couplings on the filter body and noise induced in the sensors above 100 Hz. (Kenjii Numata measurement for the TAMA interferometer [4])

Until the present work, because of this high frequency saturation, there was no way to overcome the 60 dB (that is 3 order of magnitude) limit in vertical attenuation.

2.4 The Inverted Pendulum (IP)

The attenuation limitations (saturation) of the IP are completely analogous to those observed in the GAS blades. It is important to understand how the problem arises and how it is solved in the IP legs.

The inverted pendulum is the solution adopted by SAS as passive mechanical filter for the horizontal motion.

An inverted pendulum. (IP) is a horizontal pre-isolation stage with ultra-low resonant frequency (below 100 mHz). The IP is implemented in the SAS, to achieve three main objectives:

- To provide sufficient attenuation at frequencies of the micro seismic peak (the one due to the ocean activity about 100 mHz to 300 mHz);
- To realize a mean to position the entire system, with a load of hundreds of kilograms, without requiring large force;
- To provide a stage on which to detect the recoil and actively damp the motion of the suspended chain.

To achieve these aims, the IP is implemented using an elastic flex joint counteracted by a gravitational anti-spring.

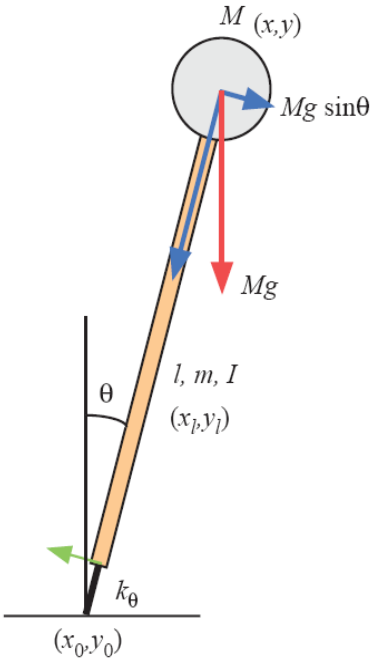

Schematic view of IP

The Euler-Lagrange equation of motion is derived as:

$$\left(M+\frac{m}{4}+\frac{I}{l^2}\right)\ddot{x}+\left(\frac{m}{4}-\frac{I}{l^2}\right)\ddot{x}_0=-\left[\frac{k_\theta}{l}-\left(\frac{m}{2}+M\right)g\right]\frac{x-x_0}{l}$$

in the first order, and it has the form of the equation of motion of a harmonic oscillator, with an effective spring constant

$$k_{eff} = \frac{k_\theta}{l^2} - \left(\frac{m}{2} + M\right)\frac{g}{l}$$

The first term of k_{eff} corresponds to the elastic restoring force of the flex joint, while the rest represents a repulsive force, so called *gravitational anti-spring* force. With the gravitational anti- spring effect, the resultant spring constant of the joint is effectively reduced. The effect of the anti-spring is proportional to the mass of the leg and the payload and can be tuned by changing the payload.

k_θ can be replaced by a complex spring constant $k_\theta\ (1+i\Phi)$ to impose energy dissipation with the loss angle of Φ in the flex joint.

Assuming the momentum of inertia of the leg being $I \sim ml^2/12$ one gets the transfer function between the ground and the payload as

$$H_{IP}(\omega) = \frac{x}{x_0} = \frac{k_{eff} + \left(\frac{m}{4} - \frac{I}{l^2}\right)\omega^2}{k_{eff} - \left(M + \frac{m}{4} + \frac{I}{l^2}\right)\omega^2}$$

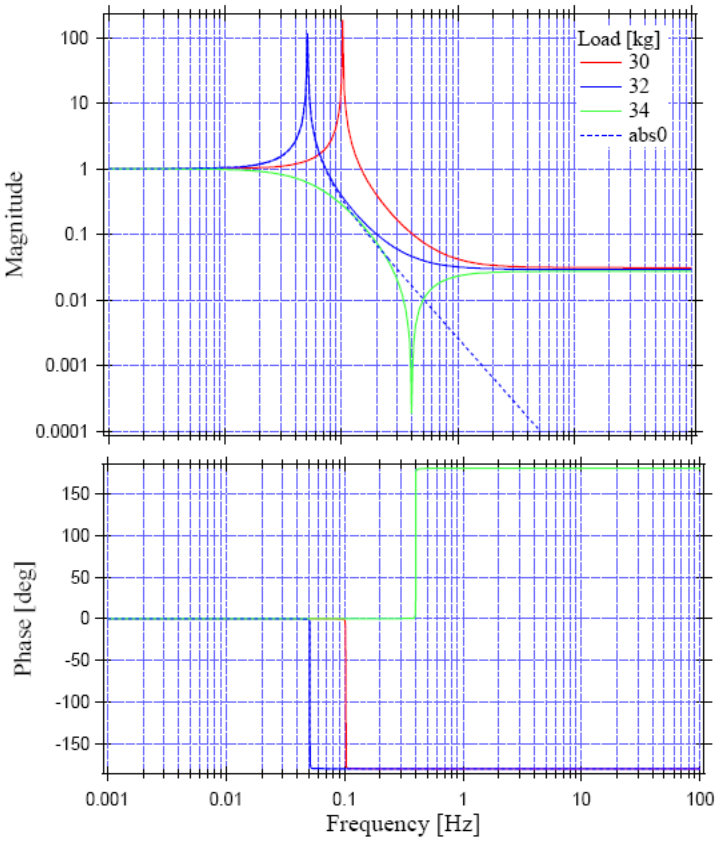

TF and its phase of the IP evaluated for different payloads and confronted with the ideal massless leg pendulum

The transfer function of the IP behaves similarly to that of the harmonic oscillator up to somewhere above the resonant frequency. While the ideal, massless oscillator shows infinite capability of attenuation, the IP transfer function saturates at a certain level of attenuation, the 'plateau'. This behavior is physically related to the 'center of percussion (c.o.p.) effect'.

When an external force is applied onto a free rigid body, it accelerates both translationally and rotationally around its center of mass. However a rigid body like the IP leg, is not allowed to rotate freely as it is connected to the payload at one end and to the ground by the flex joint at the other end. The flex joint though is a negligible constraint at frequencies higher than the resonant frequency, and the leg will rotate around a well defined point. In this case the ratio of the translational motion of the payload and the ground is determined only by the geometry of the flex joint and the center of rotation. From the equation the plateau level of the transfer function is defined as

$$H_{IP}(\omega) \xrightarrow{\omega \to \infty} -\frac{\left(\frac{m}{4} - \frac{I}{l^2}\right)}{M + \frac{m}{4} + \frac{I}{l^2}}$$

2.5 The Solution of the Problem for the IP

A way to cancel the c.o.p. effect is to provide the leg with a counterweight below the elastic joint to move the percussion point at the height of the hinging point of the flexible joint.

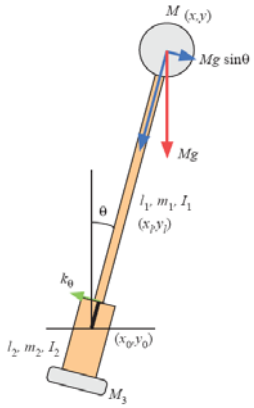

Counterweighted IP. The c.o.p. is displaced to the ground level.

In the model with the added counterweight the transfer function has the form:

$$H_{IPCW}(\omega) = \frac{A + B\omega^2}{A - C\omega^2}$$

which gives the following Bode plot:

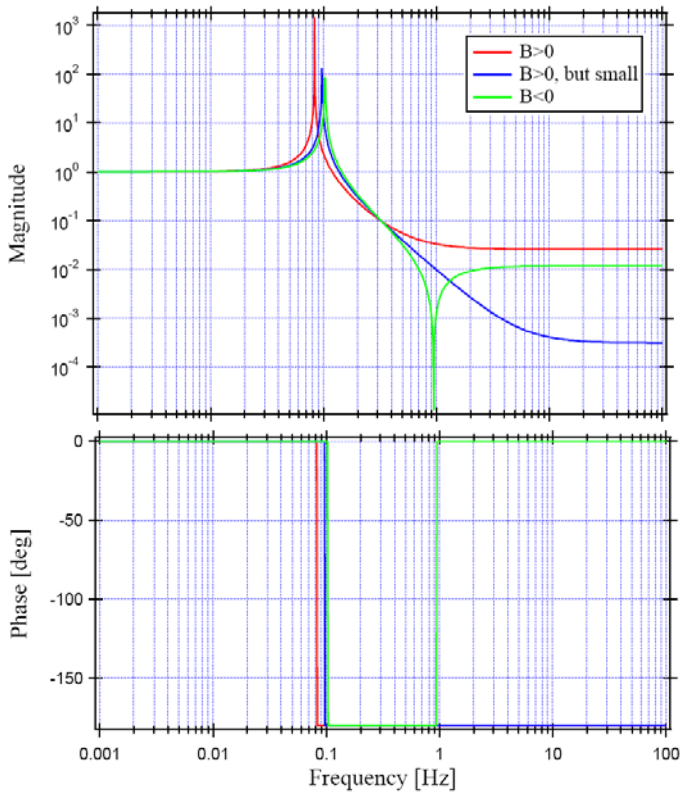

TF for the counterweighted IP. Tuning B lets to restore the massless leg pendulum

The plateau level in the transfer function is determined by *B* and *C*. The parameters related to the CW can be used to tune the maximum attenuation at high frequencies and higher attenuation levels. Particularly the IP realizes ideal attenuation when *B* is made null with the optimal CW. Too much CW over-compensates the mass of the leg and brings the center of percussion point below the flex joint, then the IP leg rotates in differential mode with respect to the translational motion. The tip of the leg moves in the opposite direction of the perturbation motion and a notch appears in the transfer function. At this point the phase of the TF changes sign (180^o rotation).

The counterweight makes the IP leg virtually massless and, in principle, completely eliminate the attenuation saturation due to the COP effect.

Unfortunately the blades of the GAS filters are flexible and cannot be equipped with a suitable counterweight. For this reason it was believed that the GAS filter 60 dB attenuation saturation was an unavoidable limitation.

Chapter III

THE SOLUTION FOR THE GASF

Taking inspiration from the successful counterweight idea which solved the attenuation saturation problem for the inverted pendulum, we looked for a solution to be applied to the GAS filter. The main subject of this thesis is about the efforts made by the author to achieve this result during the summer 2005 at the LIGO-SAS laboratories of the California Institute of Technology in Pasadena.
Qualitatively we can say that the saturation limit of the transfer function at high frequencies is due to the distributed mass of the blade springs which makes their moment of inertia be relevant when they fold up and down following the payload oscillations. Above a critical frequencies they rotate about a non well defined point and get to experience the consequences of the center of percussion effect typical of all massive extended bodies.

3.1 System design

From the inverted pendulum example we know that the effect can be compensated by moving the leg's center of percussion to the point from which the system is shaken. It was not immediate how to do that for the flexible blades that cannot be directly counterweighted. Thence instead of acting on the blades themselves, we thought of adding a second parallel system which would produce an opposite c.o.p. effect to compensate for that of the blades.

The way we followed to generate the desired cop effects was by a rigid counterweighted rod hinged on the retainer ring. Placing the counterweight of the rod outside the hinging point it should have been possible to have the center of percussion in the position required to produce the desired compensation.

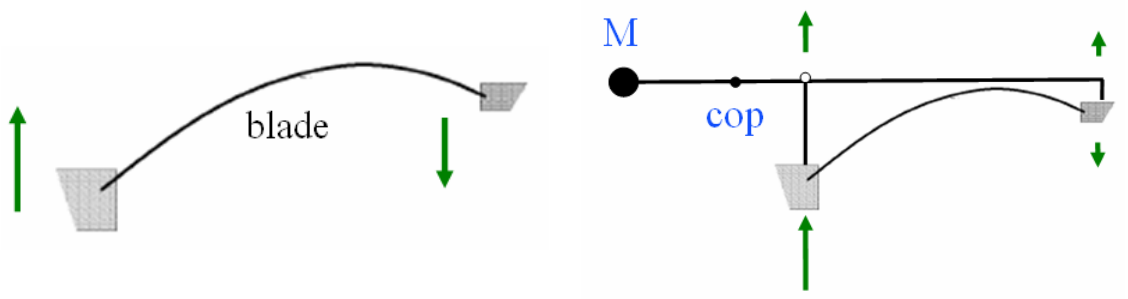

Above a critical frequency the blade, because of its distributed mass, behaves as a rigid body and rotates around its center of percussion. The added wand, because of the outer counterweight with respect to the shaking point, can introduce a negative c.o.p. effect in principle able to compensate for that of the blade spring.

We designed a horizontal wand to be mounted between the filter blades, hinged between the retainer ring and the central disc of the crown of blades. This wand has a similar shape as the one of the inverted pendula and introduces the same inertial compensation effect. The hinges are made as soft as possible to introduce the smallest possible elastic perturbation to the GAS spring. The wand is made as light as possible to avoid positive contributions to the COP effect.

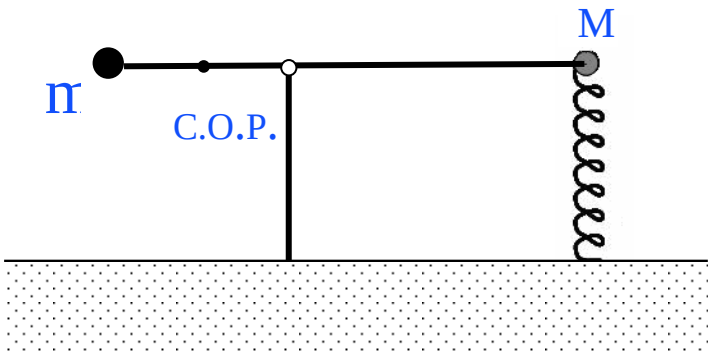

A very simplified model of the MGASF with the wands implemented can be made with a counterweighted rigid rod and a massive spring acting in parallel between the ground and the payload. The mass of the spring introduces the saturation of the blade springs.

We constructed a prototype made of a carbon fiber pipe 35 cm long. The choice for the carbon fiber and the pipe shape were made to provide rigidity and high resonant frequencies of the leg vibration modes. Thin 1.5 mm walls minimize mass and moment of inertia which can become a bypass route transferring seismic noise to the suspended load.

The tunable counterweight was achieved by tuning nuts along an outer brass threaded tube glued on the outside end of the pipe.

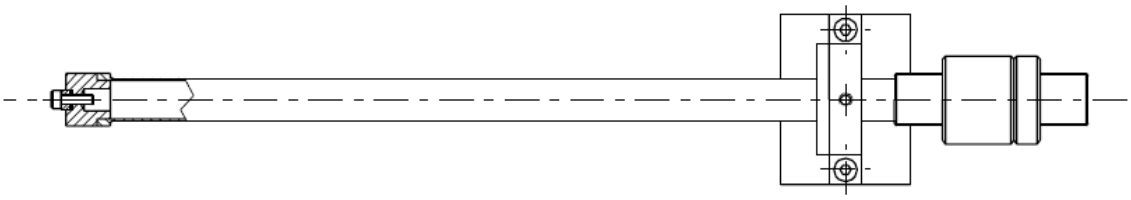

Sketch of upper view of the wand constrained to the joint system. At the right end is the brass support for the counterweight.

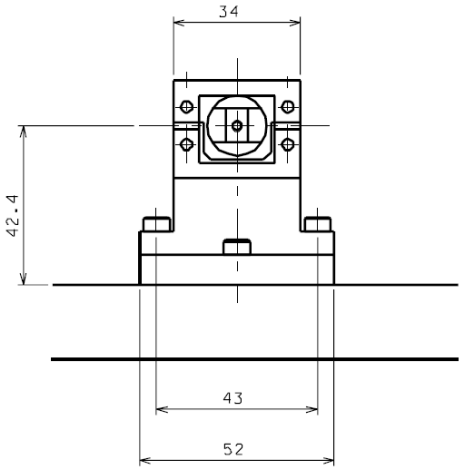

Drawings of the joint complex which sustains the wand allows it to rotate.

The carbon fiber wand constrained to the aluminum slab.

Complex joint containing two steel springs.

The wand clamped to the blades' retainer ring.

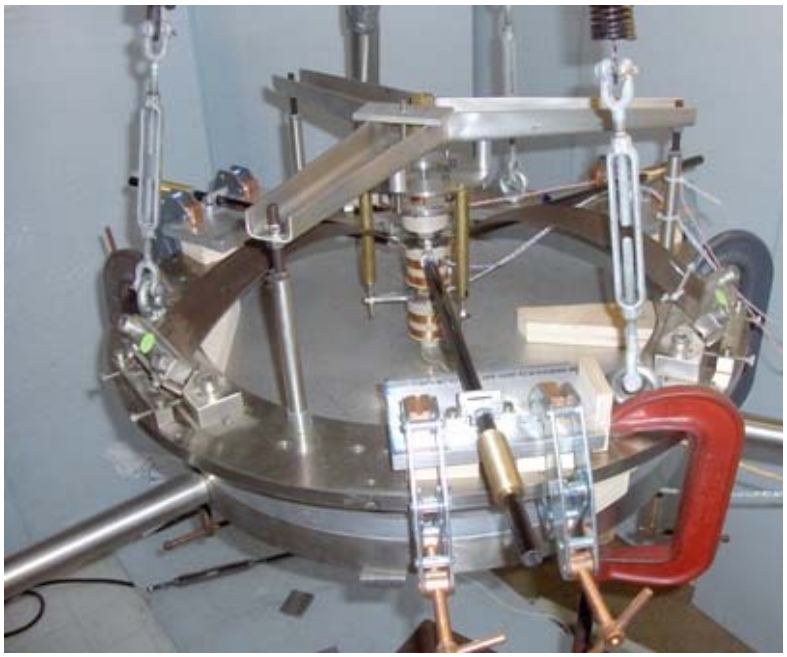

The three wands connected. Here the ring is clamped to the ground frame

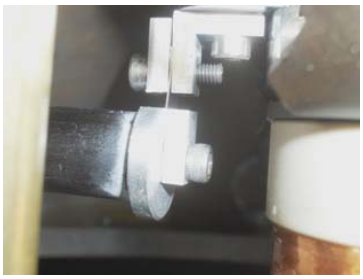

The joint hinging to the blades.

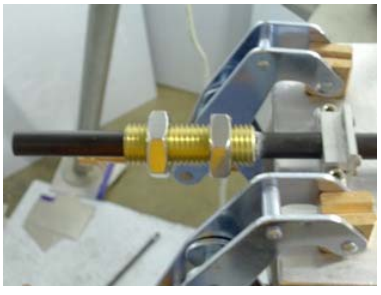

Brass counterweight support.

Chapter IV

THE EXPERIMENT

4.1 Measurement apparatus

We studied the performance of the compensating wand measuring the transfer function of the GAS filter to oscillations of the blade base provided by an excitation system. Basically this apparatus consists of a mechanical frame sustaining the GAS blades retainer ring by three garage springs. The force actuator was a loud speaker on the top which shook the filter through a coaxial rigid pyramidal system of rod. The symmetry was essential to avoid the measurement perturbation due to the motion of the system along other degrees of freedom than the vertical one.

The speaker was driven by a suitably amplified signal provided the spectrum analyzer.

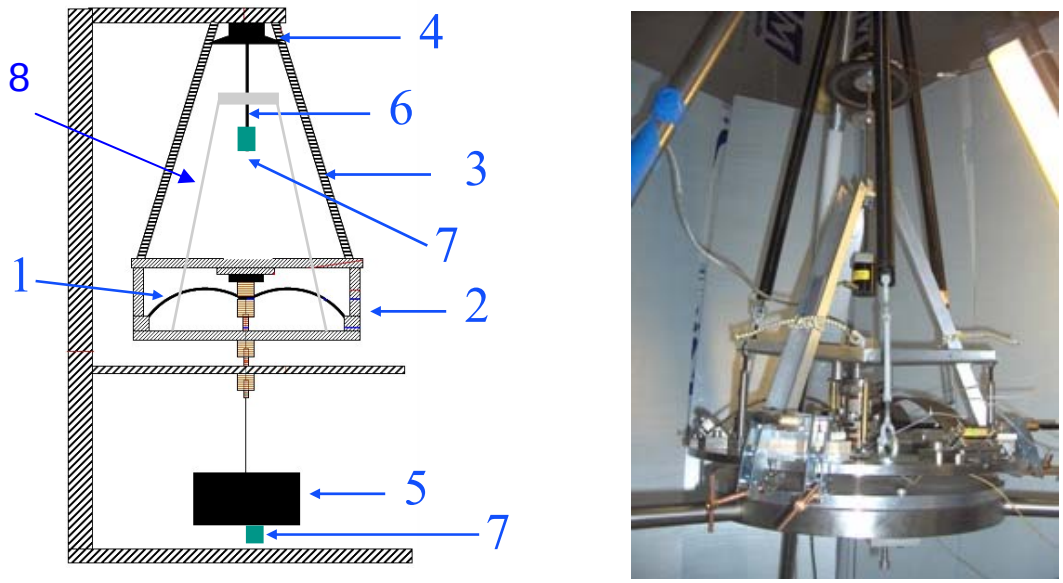

Scheme of the excitation system: 1) GAS blade; 2) Filter body; 3) Support spring; 4) Voice-coil; 5) Payload; 6) Rigid connector; 7) Accelerometer; 8) Rigid pyramidal connectors.
All the apparatus was enclosed inside an isolation chamber to protect it by the air movement and to provide thermal isolation.

4.2 Spectrum Analyzer

The Frequency Response or Transfer Function H(ν) of a linear system can be represented as the complex ratio of the system's output to its input in the frequency domain:

$$H(\nu) = \frac{O(\nu)}{I(\nu)}$$

The way to measure H(ν) by hand is applying inputs I as sinusoids of various frequencies ν and measuring the output magnitude ratio and phase difference with respect to the input. A FFT (Fast Fourier Transform) Spectrum Analyzer carries out an equivalent procedure. Exciting the system with noise of many frequencies the analyzer calculates the Fourier transforms of the input and output, then forms the ratio O(ν)/I(ν) to determine the frequency response.

At each frequency point, the input measures the amount of signal at the source frequency. This is done by multiplying the input data by the source sine (and cosine) and averaging the results over an integration time. The actual integration time is always rounded up to an exact number of cycles of the source frequency. This rejects signals which are at different frequencies, such as noise and harmonics. Long integration times improve signal to noise while increasing the measurement time.

The choice for the power of the source had to be done for every frequency interval. Greater source signals turned out into greater output signals. The effects were a better signal-noise ratio at low frequency and a worse ratio at high frequencies. In fact most of the mechanical parts have high natural frequencies that produced more noise when excited with more power.

phase jump corrections

The spectrum analyzer provided phase values of the transfer function in the range between -180° and +180° degrees. Because of that it was not a trivial issue to understand the actual trend of the phase. For instance, when the phase overcame -180° it appeared as a jump to positive values even if there was any actual discontinuity. In some circumstance it was obvious what was the actual trend and we could correct the date to restore it. In others, mainly in presence of much noise, the operation was almost impossible.

4.3 Sensors

We used two different kind of sensors: LVDTs and accelerometers. The firsts performed better at lower frequencies and were almost useless above some tens of hertz. We used them to tune the filter resonant frequency. The accelerometers were much more accurate at frequencies higher than 100 mHz.

LVDT

An LVDT [13] (Linear Variable Differential Transformer) is constituted by three coaxial coils, two large ones in series, coiled in opposite direction, which are mounted on a reference structure and act as receiver and a smaller coil, which is the emitting coil, positioned between the larger two and fastened to the moving mechanical component.

The central emitting coil is driven by a sinusoidal signal with frequency between 10 kHz and 20 kHz. The coils are made in Kapton-coated copper wire wound around a peek support. The position measurement is obtained by measuring in a lock amplifier the amplitude and sign of the voltage generated in the receiving coils by the little emitting coil. Obviously the measured voltage depends on how the magnetic field of the two coils overlap and the right choice of the geometry permits a 1% linearity over a region of a few centimeters at low gain. At high gain the readout range is strongly reduced to improve the sensitivity to a nm.

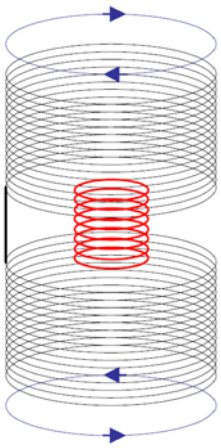

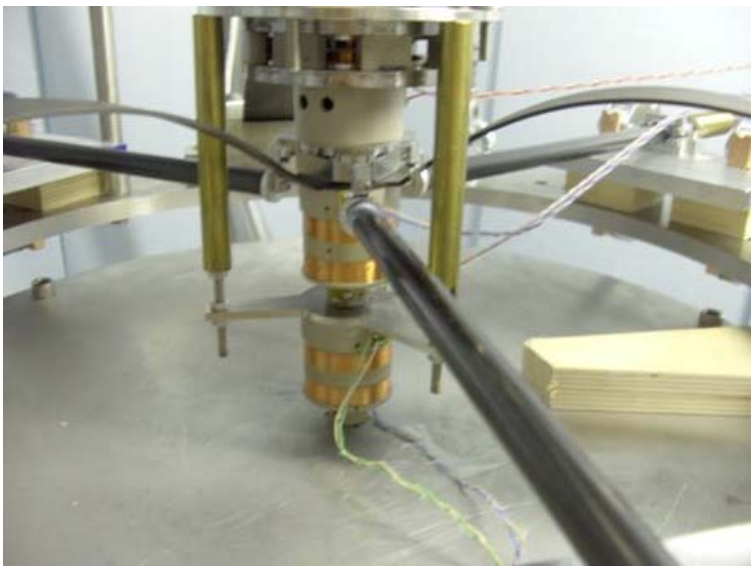

Left: Schematic drawing of the LVDT. The small red coil represents the excitation coil and the black big coil represents the two receiving coils wired in series. Right: payload-plate LVDT on top, plate-ground on bottom

Accelerometers

These sensors give a signal proportional to the acceleration that, in the harmonic motion description, result proportional to the displacement multiplied by the angular frequency squared. In the ratio between the output and the input sensor signals the angular frequency terms cancel, leaving the motion TF of the signal.

We used piezoelectric accelerometers which are based on the property, exhibited by certain crystals, that a voltage proportional to stress is generated across the crystal.

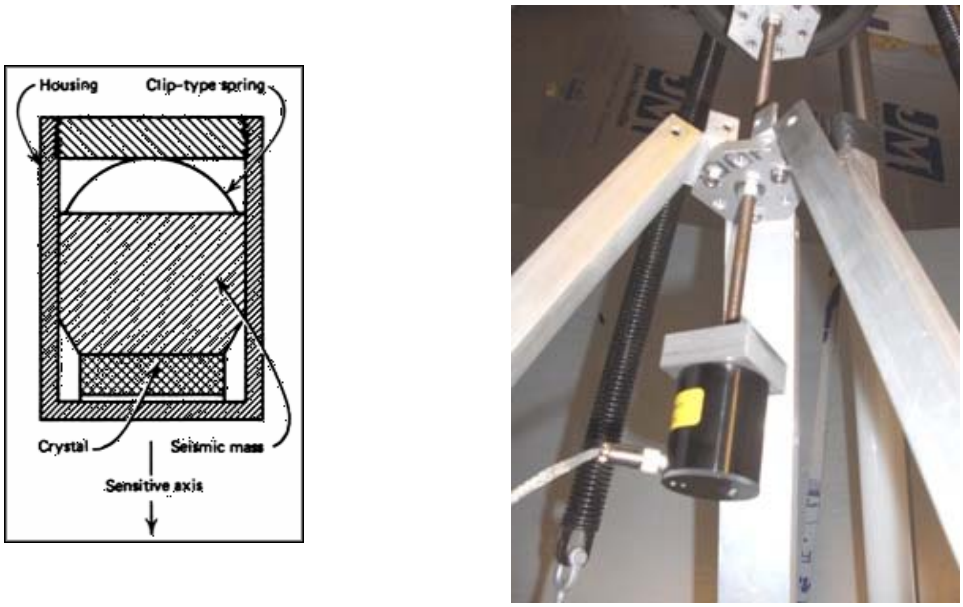

A piezoelectric accelerometer scheme (left). The TEAC accelerometer used for the input (right).

A piezoelectric crystal is loaded with a test mass glued in contact with one crystal surface while the opposite surface is fastened to the system to be measured. When exposed to an acceleration, the test mass stresses the crystal by a force F = ma, resulting in a voltage proportional to the acceleration generated across the crystal. A measure of this voltage is then a measure of the acceleration. The small variations of voltage are measured in the form of a variation of charge over the rather large crystal capacitance. For this purpose a specialized charge amplifier is used, that correct for the dynamic nonlinearities introduced by the crystal elasticity.

In our setup, at high frequency, the input accelerometer became more sensible to the vibrations coming from the speaker through the air than to that propagating directly

trough the rigid connector. This was always a cause of a significant acoustic noise which most of the time invalidates the measurement of the TF and its phase at high frequency.

Measuring a transfer function with accelerometers it is fundamental to ensure they give same outputs amplitude for same inputs. If for instance one is amplified by a constant factor α and the other by β, and $\alpha \neq \beta$ the TF might be shifted:

$$H(\nu) = 20 \cdot \log \frac{\beta \cdot O(\nu)}{\alpha \cdot I(\nu)} = 20 \cdot \log \frac{O(\nu)}{I(\nu)} + 20 \cdot \log \frac{\beta}{\alpha}$$

If neglected, this effect introduces a systematic error in the measurements. Even if the driver device tries to provide same amplifications to both sensors, in order to minimize the shift term the by-hand calibration of the signals is necessary. One way to verify this operation had been done properly was comparing two measurements taken at the same conditions but with inverted accelerometers, moving input one to the output and vice versa, leaving unchanged their connections to the instruments. The two measurement should coincide only in the case there is not relative amplification between the sensors.

In our case that measurement showed a small displacement of about 3-4 dB. This means that the actual measurement has a systematic error of this factor.

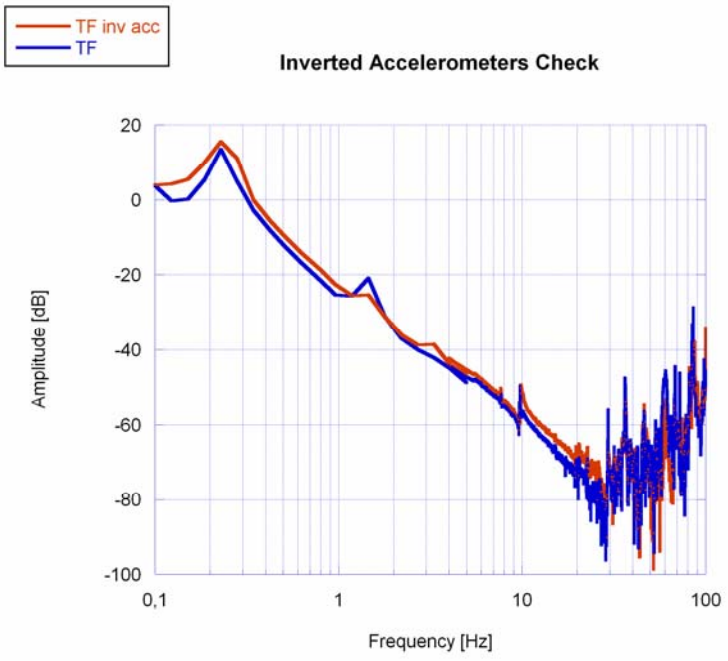

Inverted accelerometers check. The 3-4 dB shift is a systematic error in the measurements.

Unless differently specified, the measurements presented in this thesis were obtained with the accelerometer set to give the higher values of the TF, that is they are to be considered at the upper bound of the systematic error band which is the pessimist case in the uncertainty range. The best way to correct it would probably have been to measure the relative transfer function between the accelerometers once for ever (i.e. placing them on the same input support, like on the plate over a shaker). Then every measured TF should have been multiplied by that.

4.4 Experiment Procedure

The attenuation performance of the GAS filter improves for a resonant frequency as lower as possible, that is when the $1/f^2$ fall starts for lower frequencies. Given the high frequency limitations of our measurement apparatus, the lowest possible resonant frequency uncover the widest high attenuation frequency region.

The GAS springs potential energy dependence to the displacement changes according to the effective stiffness of the springs. Tuning the anti-spring effect by changing the compression of the blades can, in principle give arbitrarily low resonant frequency. Above a critical compression, just after the resonant frequency nulls, the system becomes bistable. Well before that point though (at ~200 mHz), because of material hysteresis, the system becomes unstable

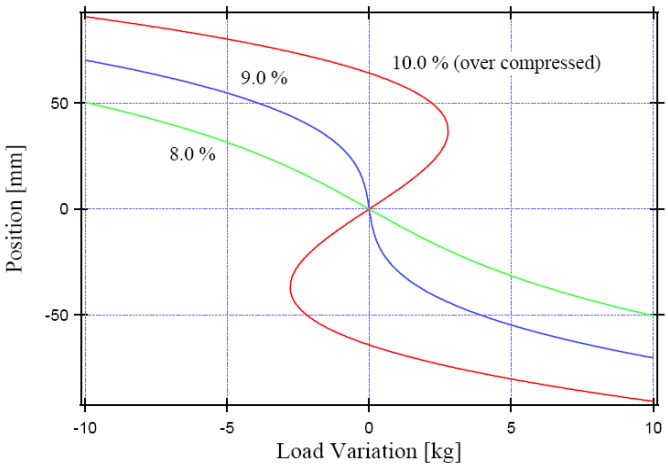

Change of the equilibrium position due to a variation of payload obtained by a GAS simplified mathematical model evaluated for a determinate set of realistic parameters. A red curve correspond to over-compression, and the system has three point where the stiffness reduce to zero.

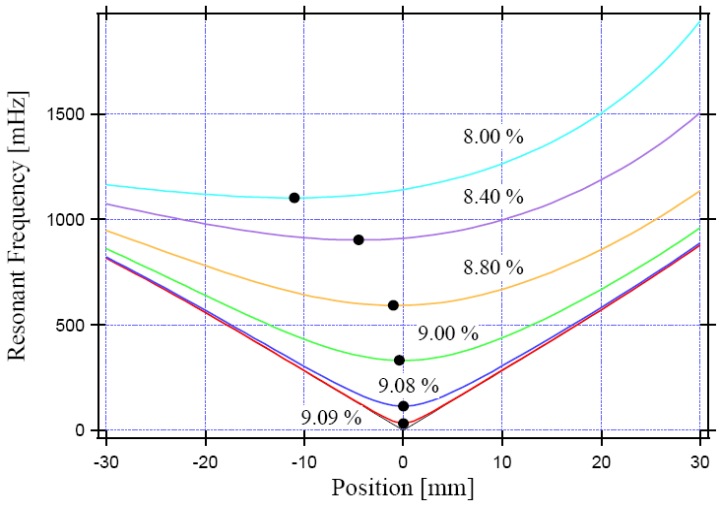

Resonant frequency of the blade with various compression factors. For each point on the curves, the payload is chosen to set the desired working position. Black dots mark the optimal working position with each compression factor.

Adding the wands to the GAS filter changed the effective elastic constant of its springs because of the additional flex joints stiffness. The counterweight of the wands also changed the GAS filter optimal loading weight.

We determined the new GAS filter best working point by tuning the compression of the blades and adjusting the ballast on the payload.

Once the compression of the blades was fixed just before the instability, the dependence of the resonant frequency versus working point height, as the payload is changed, was approximately parabolic. This measurements were done dropping small ballast on the payload. The LVDT gives as output a signal proportional to the height of the suspension point, that is monotonic with the increasing mass of the payload. The measurement of the induced oscillations gave the resonant frequency.

Frequency and voltage measurements were always taken by a digital oscilloscope on the LVDT signal.

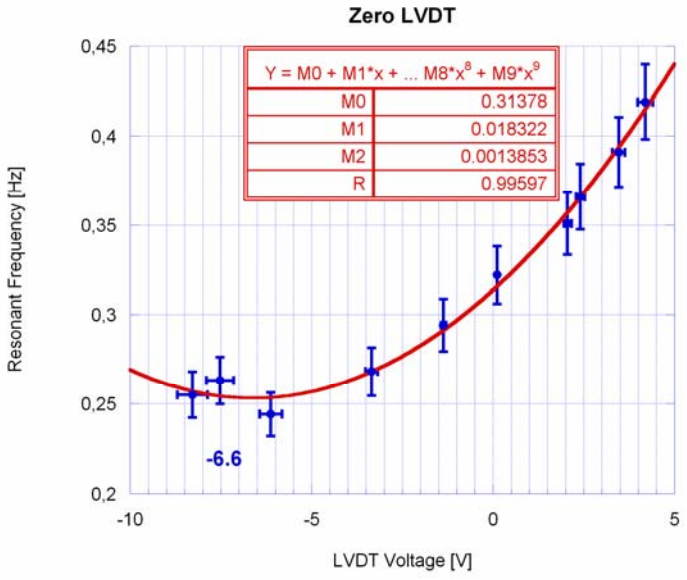

LVDT position after the end of the oscillation vs. resonant frequency

Chapter 5

EXPERIMENTAL RESULTS

5.1 Interpretation of the Measurements

The measurements discussed in this thesis are mostly shown according to the chronological order used in the quest for the best compensation of the c.o.p. effect of the GAS springs and the lowest attenuation saturation limit.

The addition of an excessive corrective c.o.p. effect to the system, as explained in the chapter 4 overcompensates the saturation limit and introduces another saturation limit, analogous to the one that we want to eliminate, but with opposite sign, and a notch in the transfer function when the $1/f^2$ transmission and the corrective c.o.p. effect have the same amplitude and interfere destructively. Ideally it should be possible to restore the $1/f^2$ trend over all the frequencies at the transition between undercompensation and overcompensation. Our purpose was to set the system in the condition where it shows the lowest saturation limit.

Analogously to the case of the inverted pendulum, decreases in compensation (decreasing or shifting the wand counterweight closer to the flex joints) move the overcompensation notch toward higher frequencies and makes the saturation deeper.

When the system is close to the critical threshold, it is not easy to see if there is a notch in the transfer function or measure the effects of little variations. We found that the TF phase is a better and less noisy indicator of the notch position. In fact the notch, that is the interference between the unwanted and the corrective (opposite sign) forces, also implies the 180^o change in the TF phase. For this reason the measurement of the amplitude TF have always been complemented by that of its phase. Naturally, when the distance from full neutralization becomes smaller than the measurement noise level, one cannot infer definitive conclusions from the data.

Thence the way to optimize compensation is to measure the position of the notch as a function of decreasing compensation until its effects become covered by the

measurement limits of the apparatus. Then one extrapolates to the counterweight position that would move the notch to infinite frequency and sets it there. Alternatively one can look for two counterweight settings that produce the same saturation level in under- and over-compensation and set the counterweight at half way. The two methods are equivalent. We had no time to perform a complete optimization procedure and to figure out which of the two methods was more effective.

The following paragraphs illustrate a simple model of the system, followed by the progression of measurements that constitute a rough approximation of the above described strategies. These measurements were performed with purely mechanically tuned GAS filters. We found that the $1/f^2$ curve dipped too soon in the measurement noise to allow satisfactory tuning. Then we passed to measurements performed with a GAS filter where the resonant frequency was tuned below the 200 mHz limit by means of corrective electromagnetic springs [7]. The best results thus obtained are then displayed. Some surprises emerged.

5.2 The Quest for the Best Settings

1) Initial System

To study the effect of the implementation of the compensating wands, it was important to know the initial performance of the un-modified GASF.

We started measuring the transfer function of the GAS prototype as it was and we reproduced the four year old K. Numata results. Note that having no compensation the phase has no oscillations after the initial change of sign in correspondence with the main resonant frequency at 200 mHz. It is worth noting the raise of instrumental noise above 30-40 Hz and the increase of phase noise for low signal amplitude.

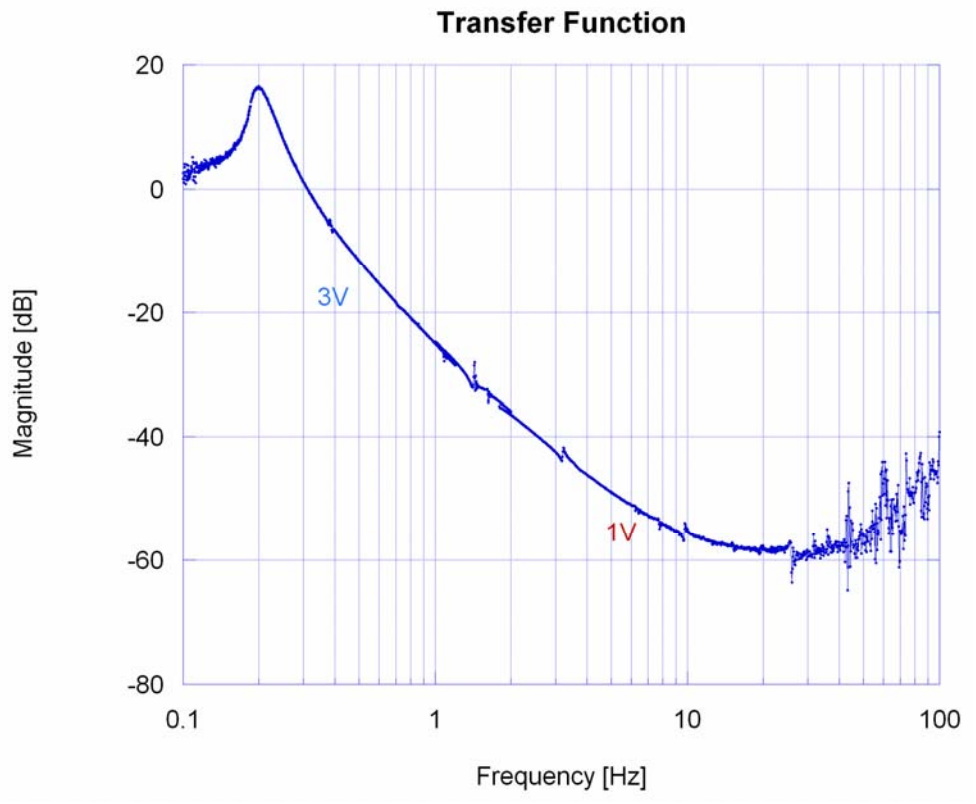

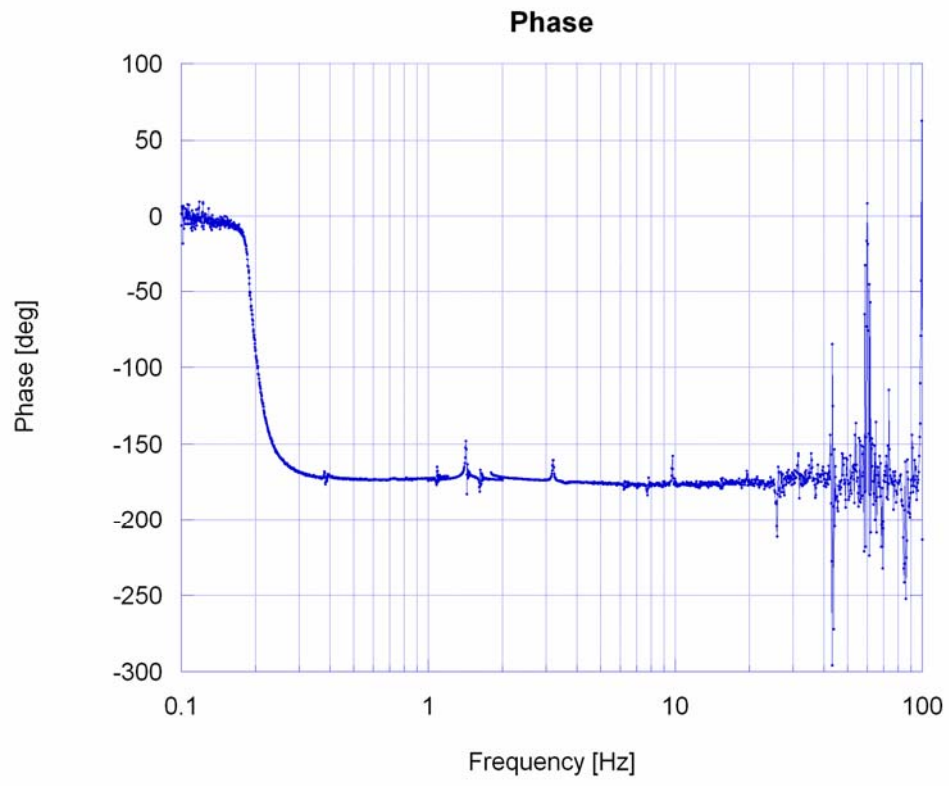

Amplitude and phase of the TF of the GAS filter as it was before adding the compensating wands. The attenuation saturates at 60 dB. Acoustic noise dominate at high frequency. 3vV and 1V are the different amplitude of the source. The peak about 1.3 Hz correspond to the resonances of the garage springs and to the pitch induced on the payload.

2) Three Wands

The second step was to implement the wands, for symmetry we had built three of them and mounted them in between the three filter blades. None of the wands had counterweight in addition to the weight of the brass threaded rod for the nuts.

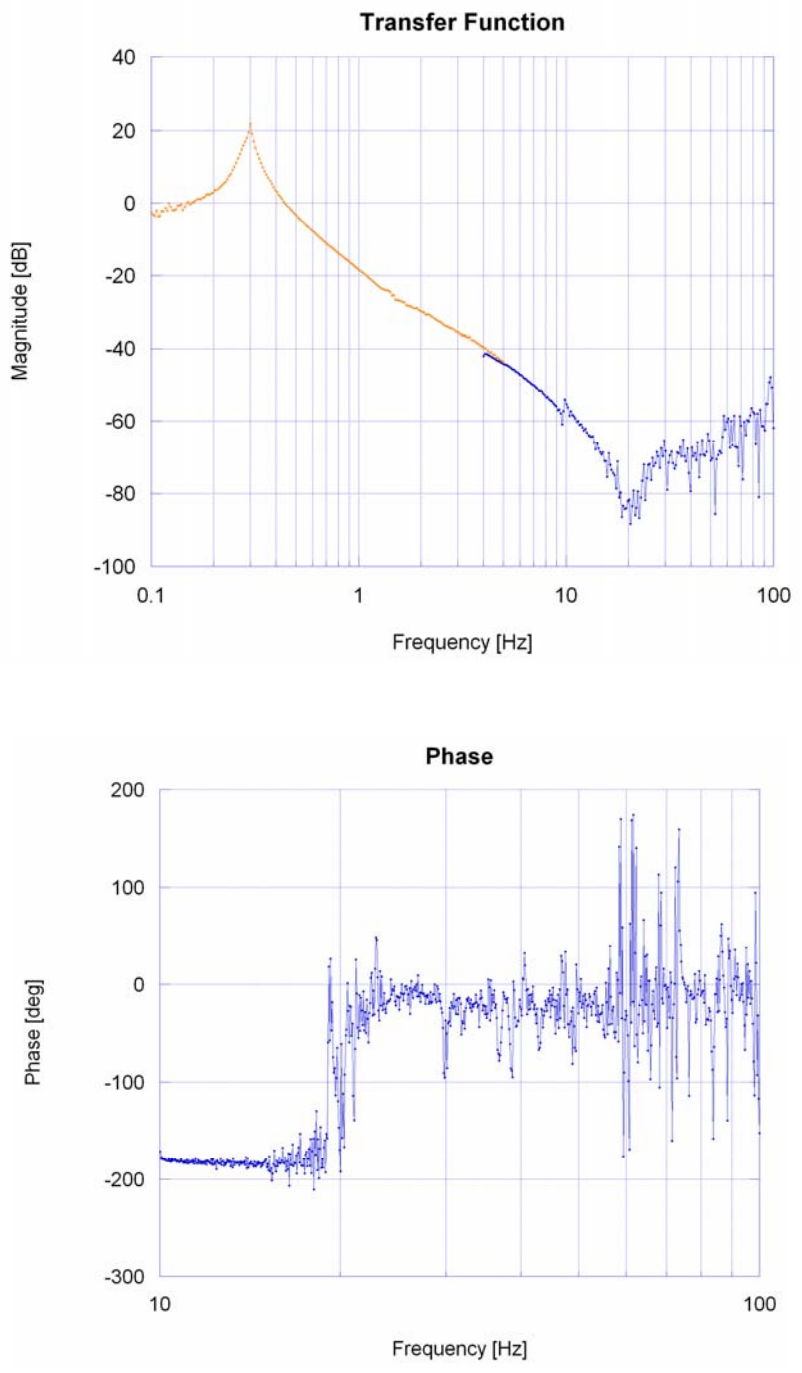

TF with three wands implemented. None carries any additional counterweight. The attenuation overcomes 80 dB and the phase flips of 180° in correspondence of the notch introduce by the external center of percussion.

Even if a calibration problem with the accelerometers applied a down shift to the entire TF (see the non-zero baseline at 0.1 Hz), the measurement is valid to see the expected effect. The acceleration calibration problem was mostly solved thereafter, limiting the systematic errors as discussed in section 4.3.

The resonant frequency of the filter was about 300 mHz. Both the transfer function and its phase show a notch and the corresponding phase flips at about 20 Hz. The system is obviously already overcompensated.

The irregularity between 1 and 2 hertz and the one about 10 hertz were common to all TF plots and independent of tuning, they are payload or measurement setup resonances. The jump at about 1.35 Hz was produced by the vertical resonance of the garage springs, which excited the pitch resonance of the payload. The resonance about 10 Hz remains unidentified.

Many of the high frequency peaks in the plot are resonances due to the mechanical complexity of the measurement apparatus.

As always, the measurement was noisier at high frequencies where the signal is weaker.

3) Three Wands each with Two CWs

To verify that the system was already overcompensated with the three naked wands, we added 2 CWs to each of them to enhance the effect. Note that the addition of mass to the wand should have lowered any of its internal modes and made them visible. None is becoming clearly visible, sign that the internal modes of the wands are not a problem.

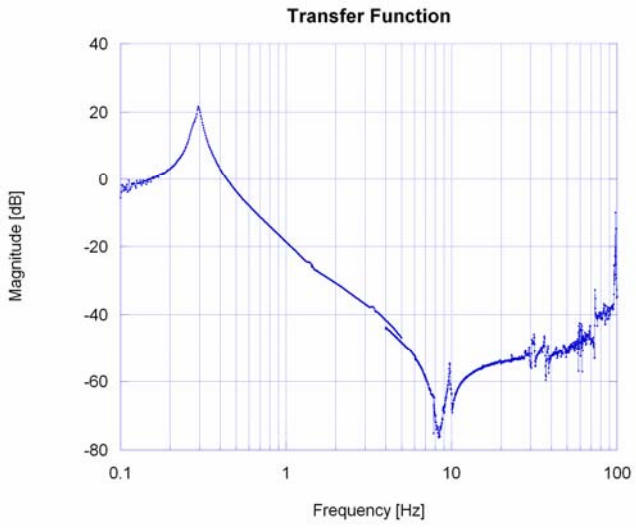

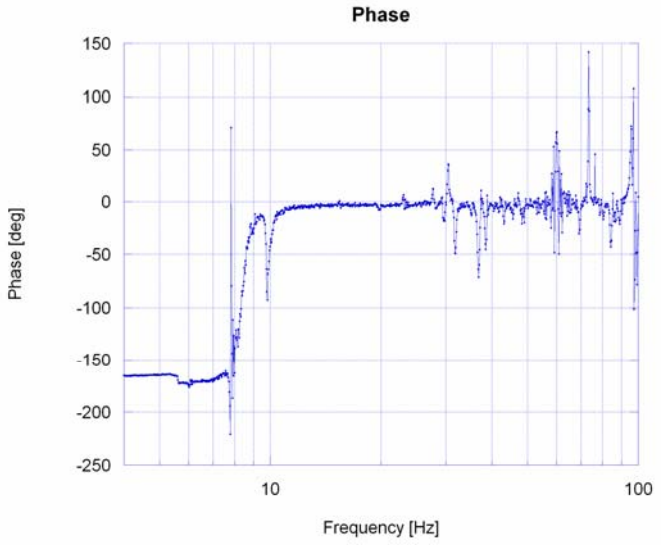

A calibration problem of the accelerometers shifted downward the entire plot. Enhancing the overcompensation with additional counterweights on every wand the notch deepens and moves toward a lower frequency (~8 Hz).

We obtained what expected. The notch became deeper and moved to lower frequencies, as shown by the phase as well. The saturation level also raised as expected.

4) Two Wands

Having demonstrated the overcompensating effect with the addiction of CW, we wanted to decrease it. We could not easily reduce the counterweight of the brass threaded rods. Therefore one of the wands was disconnected, leaving the other two working asymmetrically. The free wand was neutralized with rubber spacers.

We immediately observed that symmetry was not a fundamental requirement, thanks to the rigidity in all other degrees of freedom of the central disk of the monolithic structure of the blades.

In this case, to save time, we limited the measurement range to the high frequencies. The measurement is quite noisy because of the fast frequency scan, however from both plots the system appears to be undercompensated.

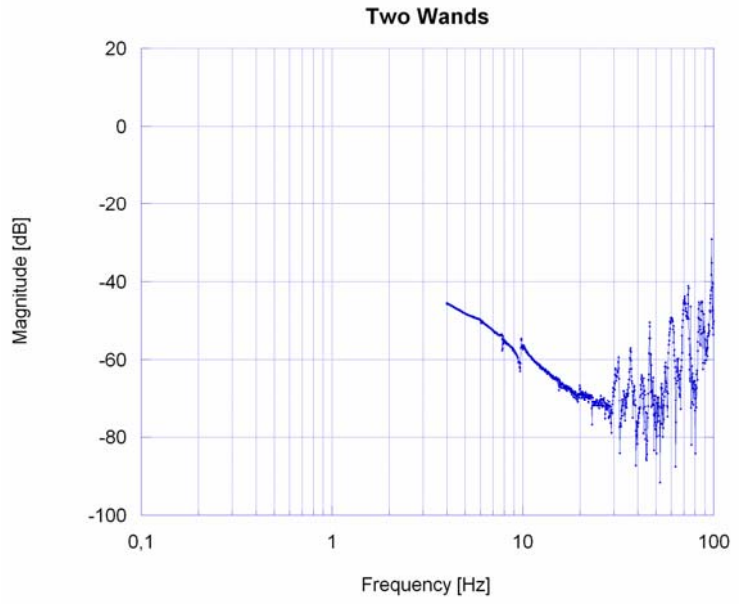

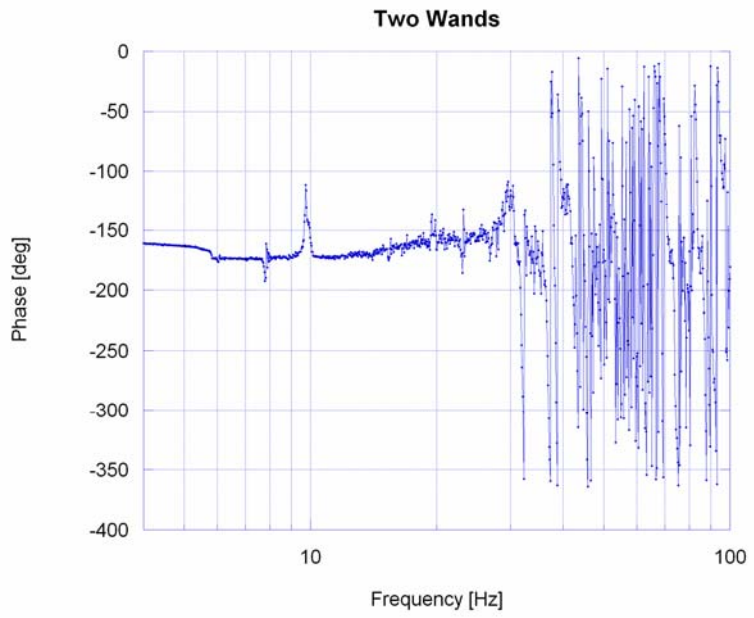

The measurement focus to the upper frequencies range. An attenuation of about 70 dB is achieved. The systems seems to be undercompensated but the noise avoids a definitive evaluation.

5) Two Wands + ½ CW

To correct for the undercompensation of the former case we added a half CW to one of the wands placing it at the inner end of the threaded rod, near the main flex joints, and then moving it to half way. Again fast measurements were performed.

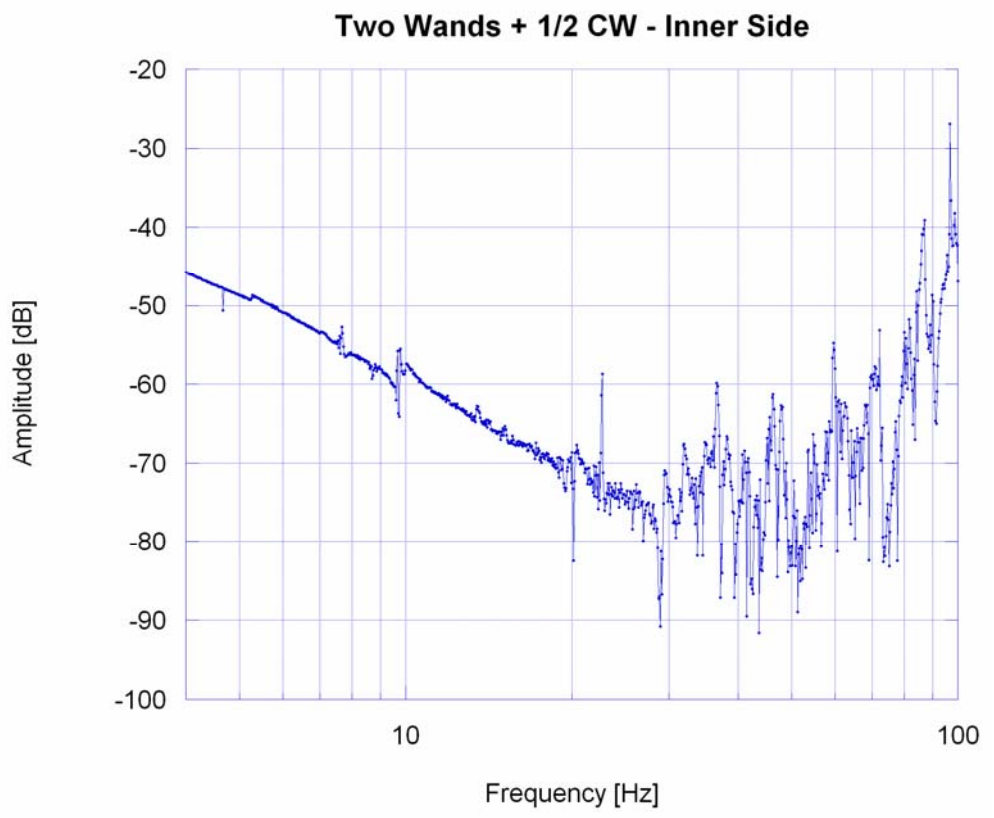

Half a nut is added to just one wand in its inner position. The attenuation improves respect with the former situation and also in this case it seems to be an undercompensation regime.

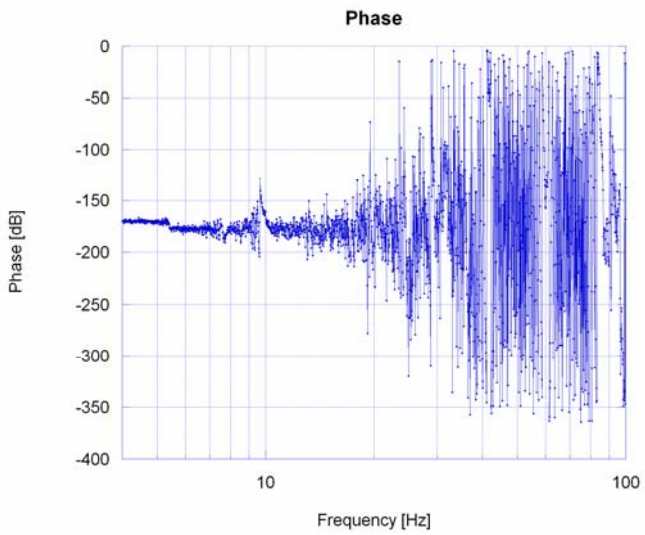

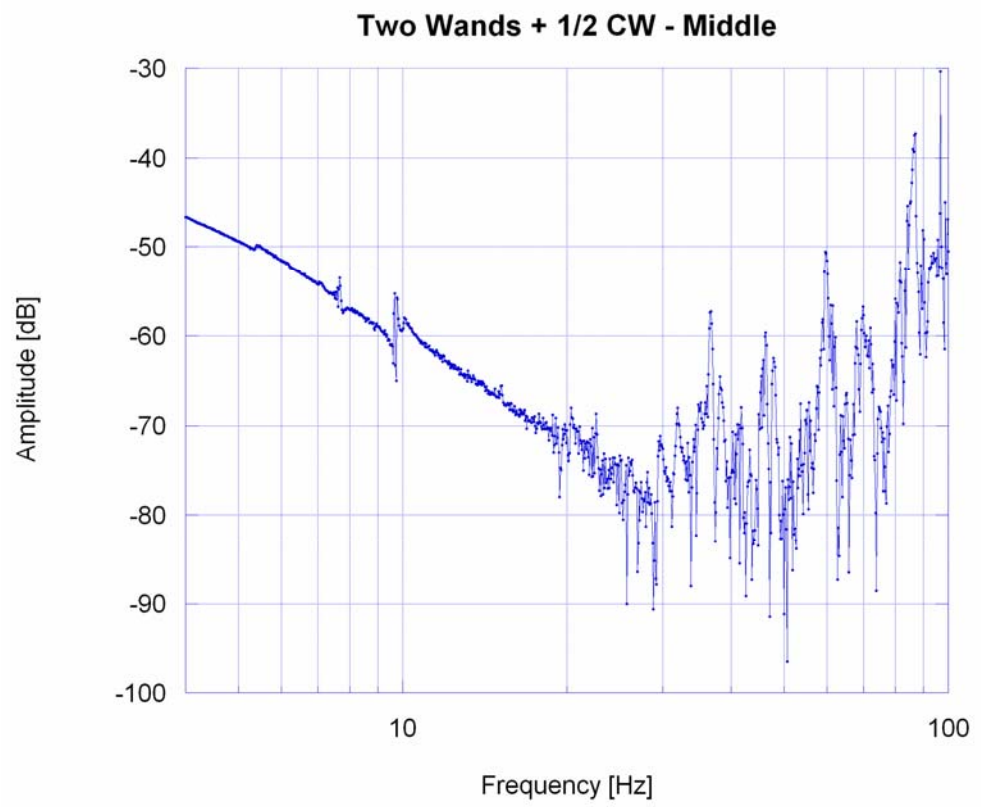

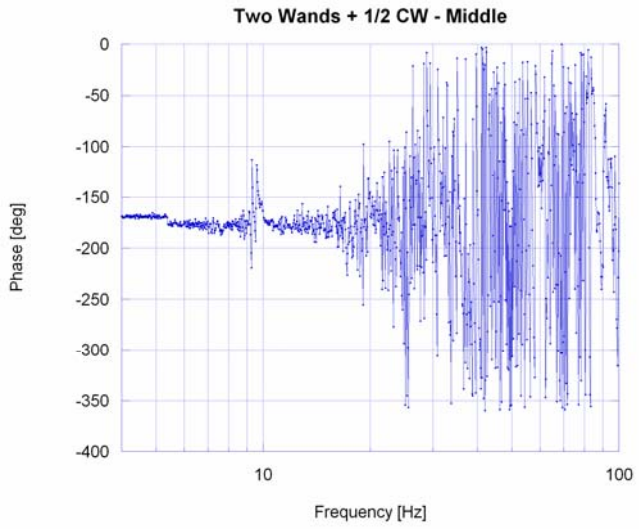

Moving the CW to an outer position seems reducing the undercompensation. Here the attenuation is higher. The noise dominates at high frequency.

The TF and its phase look quite noisy at high frequency and there is some uncertainty, but in both cases the system seems to be still undercompensated. The TF

gets to about 75 dB in the inner case and a bit more in the middle case. However this difference could also be attributed also to the variation made to the system's working point.

The achieved attenuation of more than 75 dB is definitely larger than without counterweights.

6) Two Wands 1 CW

Guessing to be still in undercompensation regime with half a CW, we tried with 1 whole counterweight nut in just one wand and examined the effects of different placements of the CW on the rod.

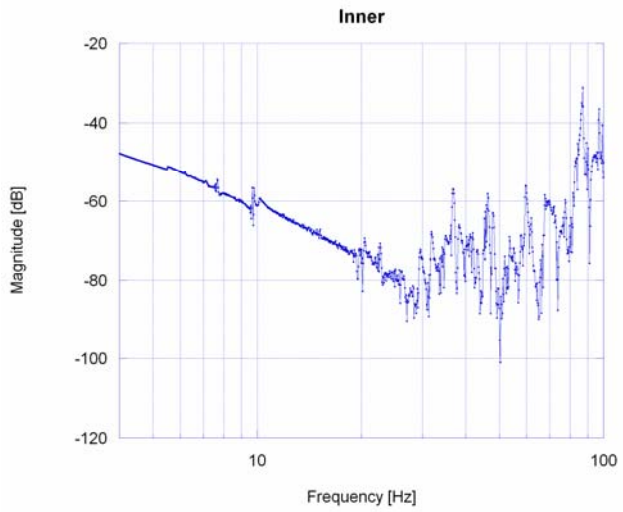

TF for the inner placement of the CW. The attenuation achieve 80 dB at 25 Hz then the noise becomes dominant.

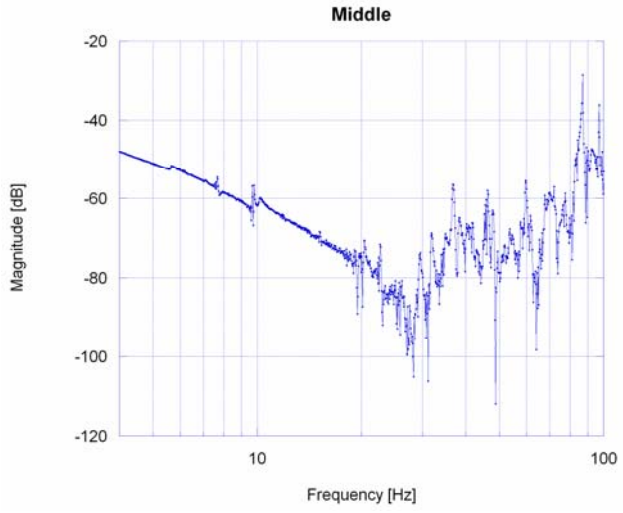

Intermediate position of the CW.

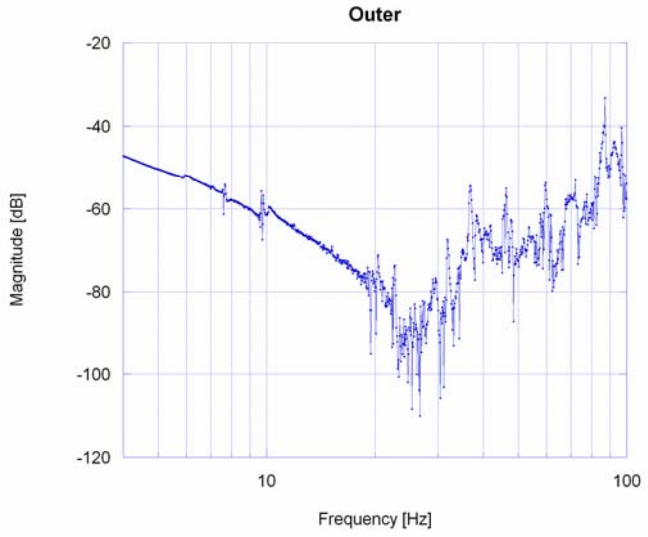

Outer position of the CW.

For all these three cases the phase was too noisy to be useful. At this stage we were taking the average of several frequency sweeps and we had not learned yet how to make the phase noise lower by making longer dwell times at each frequency instead of averaging over different measurements. Also we had not learned yet to trust the phase to optimize the tuning. Looking at the amplitude TF only, we judged that the inner was the most interesting position.

At this point we decided to work on the excitation and measurement system, to damp the high frequency noise due to mechanical resonances. We used some Velcro strips to attach masses to the rigid rods connecting the shaking speaker to the system. The expedient worked quite well.

Several 360 degrees jumps were present and clouding the phase TF. The measurement of the phase resulted clean enough to be corrected as shown in the plot in this page. The jump at about 50 Hz is attributed to overcompensation.

Note that if we extend the $1/f^2$ line to the frequency at which the phase flips we infer as much as 90 dB underlying the measurement's noise. At this attenuation level, we see appearing the resonances due to the spring effect on the wire which holds the payload and the internal blade resonances that we can't remove without adding complex dampers. The phase measurement confirmed that the inner CW positioning was the best choice with the full nut counterweight. Possibly tuning using a ¾ weight nut, or a single wand with 2 nuts would have yielded a better result (phase flip at higher

frequency). Content with the achieved result, and aware that at we could not have confirmed any further improvement of our GAS filter due to the high frequency limitations of our measurement setup, we decided to push the system to lower frequency tunings.

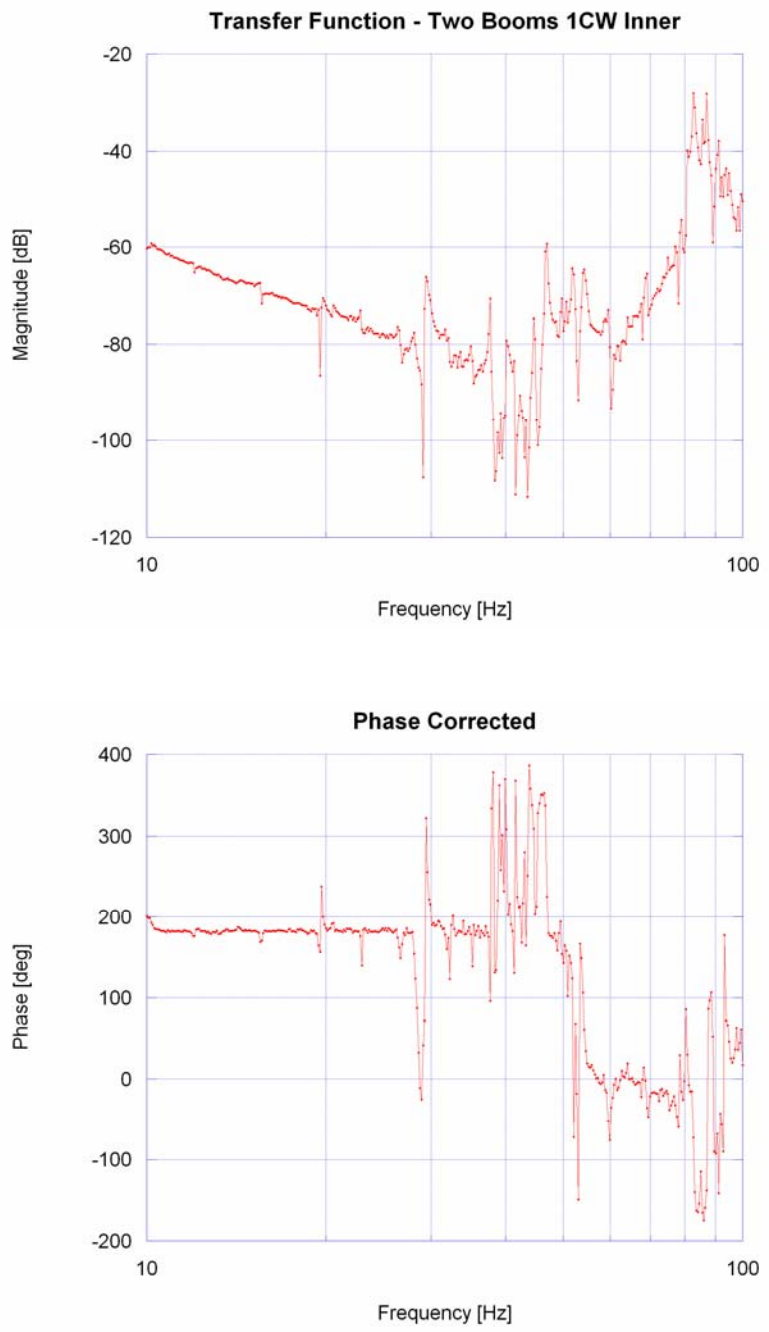

Improved measurement after damping some of the many mechanical parts of the excitation system resonanting at high frequency. The phase plot showed was obtained correcting fro the flips in the date as explained in chapter 3.

5.3 Electromagnetic Antispring Implementation

Lowering the resonant frequency of the GAS filter causes the attenuation rolloff to start at lower frequencies. As results the performance may improve, uncovering more of the attenuation saturation plateau and the measurements would look even better.

As explained in chapter 4, we cannot further compress the blades to arbitrarily lower the stiffness constant of the GAS springs because above a critical value the system becomes unstable. To avoid this mechanical tuning limit the Electromagnetic Antispring [7] had been implemented. When it is active the total stiffness of the filter is

$$K_{tot} = k_s + k_{as} + k_{e.m.}$$

where k_s, k_{as} represent the mechanical stiffness of the MGAS filter and $k_{e.m.}$ is the stiffness of the electromagnetic anti-spring.

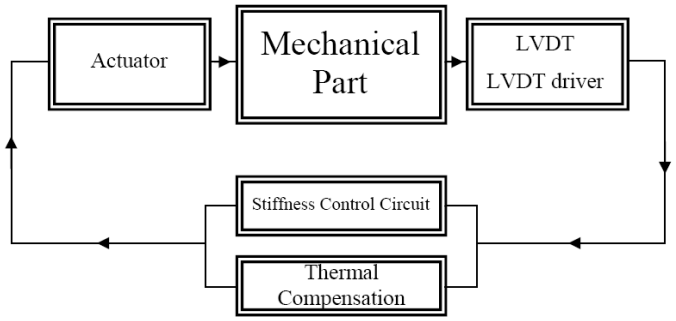

Basically the system consists of a precision LVDT position sensor coupled to an electromagnetic actuator which applies to the suspension point a force proportional to its displacement with respect to a fixed equilibrium point. By changing the gain and sign of the feedback circuit it is possible to apply a force equivalent to a tuneable strength spring or anti-spring. The proportionality constant can be tuned by hand acting directly on a potentiometer in the circuit. The system implements also a thermal compensator circuit which can correct the equilibrium point setting if it changes for thermal effect.

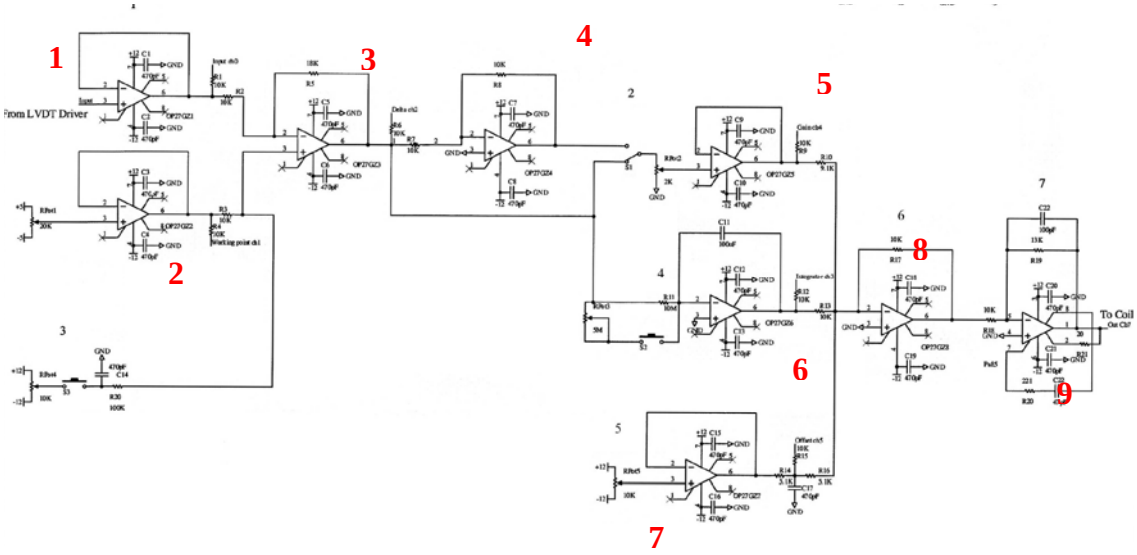

Electromagnetic Anti-Spring circuit

If we look closer to the parts of the circuit, the first two are emitter followers. The first one de-couples the signal provided by the LVDT, the second the hand-tuned offset which fixes the position of the equilibrium point. The third amplifier is a adder which actually subtracts the LVDT input from the reference offset. The forth one is an inverter that can be turned on or off depending on the desired sign of the electromagnetic spring stiffness constant. The fifth is simply an amplifier whose gain can be tuned by hand thus fixing the absolute value of the stiffness constant. The sixth is basically an integrator with a very long characteristic time, which provides nearly DC level growing or decreasing with a speed proportional to the adder average signal. It provides the thermal compensation. The seventh is an additional manual offset provider that we did not use. The eighth amplifier is a simple mixer. The ninth amplifier suitably drives the actuator coil.

The implementation of the E.M. Antispring allowed the shift of the resonant frequency of the GAS filter below 100 mHz where the accelerometers became unable to measure it. The very low frequency measurements were made using the LVDTs.

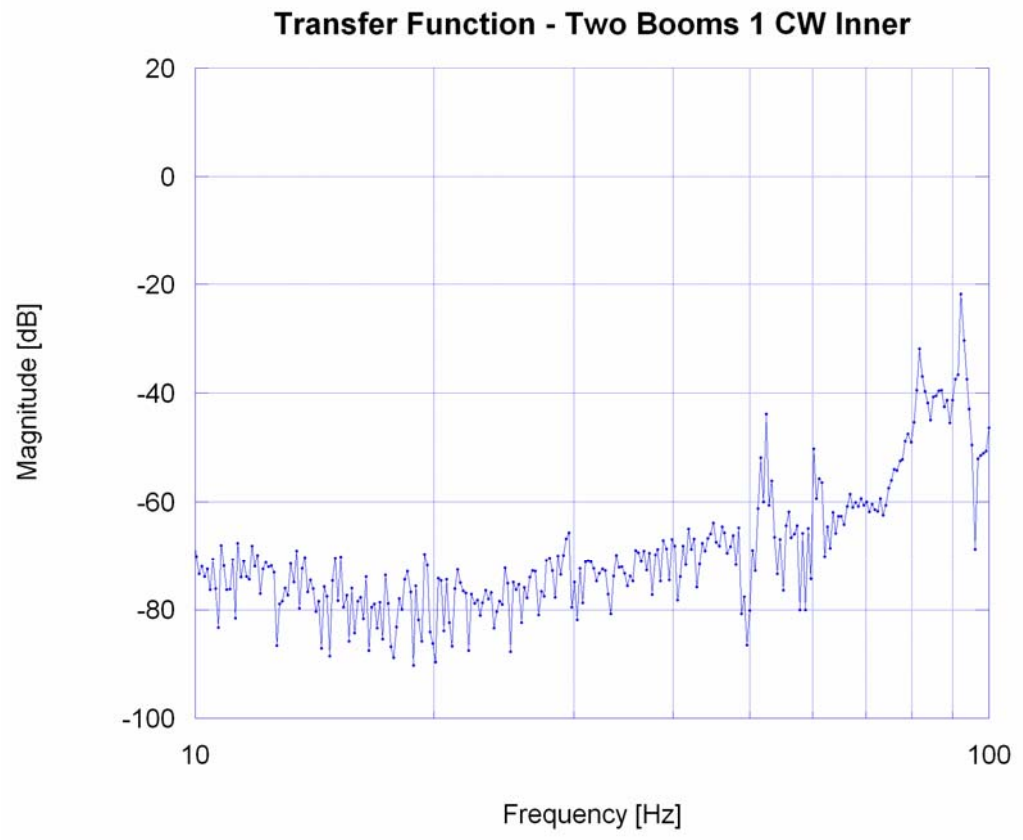

The TF zoom at high frequency is flatter and contain less noise than before the e.m. anti-spring introduction. It shows the best performance ever obtained in vertical direction by a single stage of seismic attenuator. (Boom refers to the wand, it's one of the many way we called it).

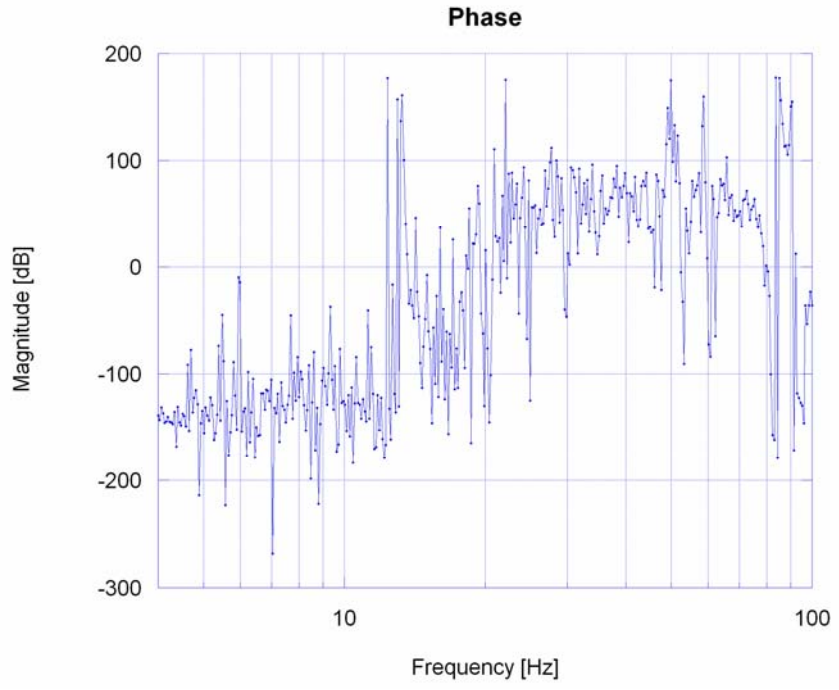

The phase confirms the overcomepensation showing a 180° flip between 10 and 20 Hz.

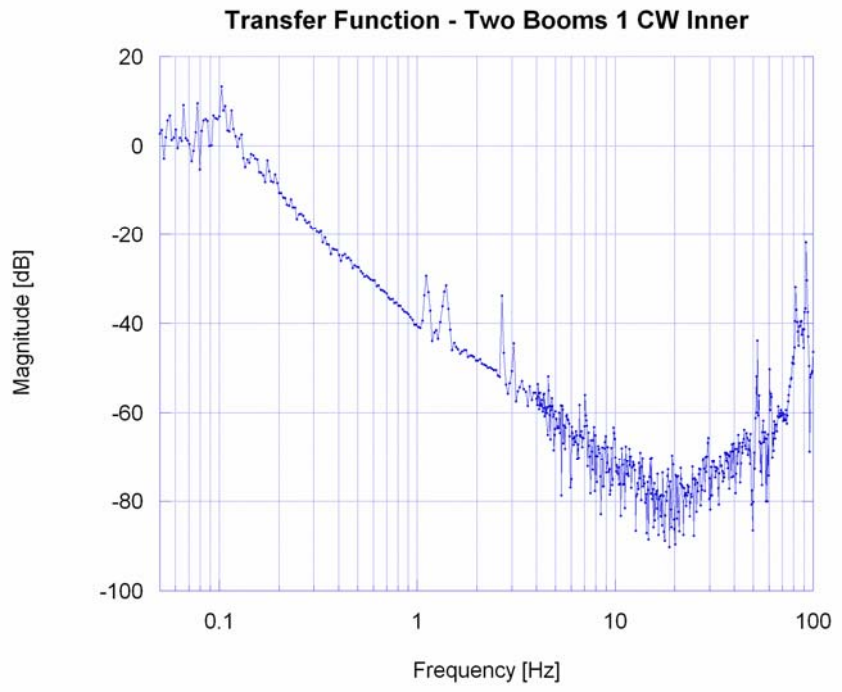

Entire TF for the case of two wands with 1 CW inner.

As expected the TF became flatter at high frequencies. The phase change sign at about 20 Hz can be associated with the notch due to the overcompensation.

Unfortunately, being based on the LVDTs, which demonstrated ineffective at high frequency, the effect of circuit is limited to the low frequency range.

Note that the above plot for the TF is the best performance ever obtained in vertical direction by a single stage of seismic attenuator.

5.4 Hysteresis

We found an unexplained deviation from the $1/f^2$ transfer function at resonant frequencies below ~100mHz.

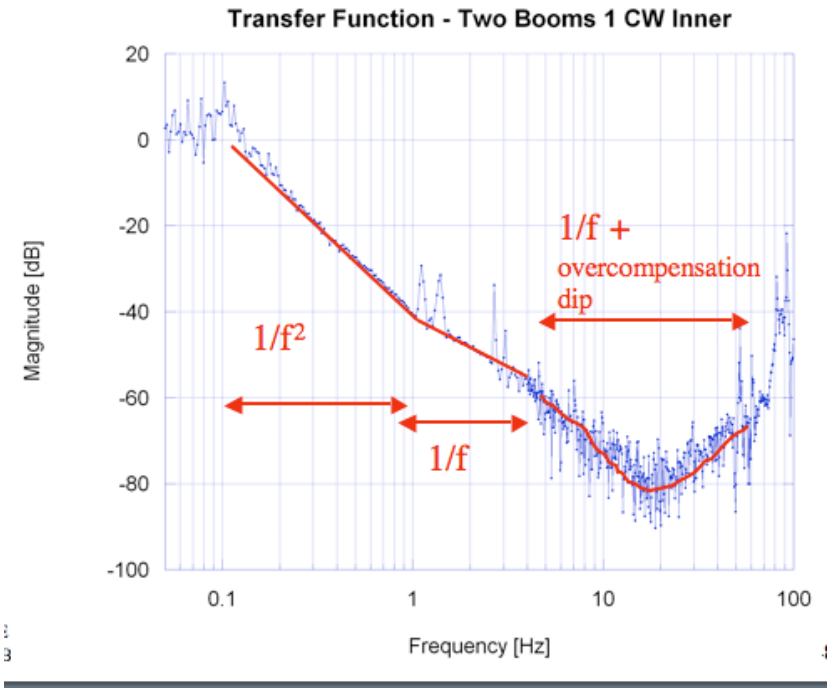

Above 1 Hz the trend deviates from the expected $1/f^2$ to a 1/f attenuation. The underlying motive is probably the material hysteresis.

It happens that, when the attenuation is very high, a 1/f trend appears instead of the expected $1/f^2$. The deviation had been already observed in the past [7], studying the gas spring at low resonant frequency.

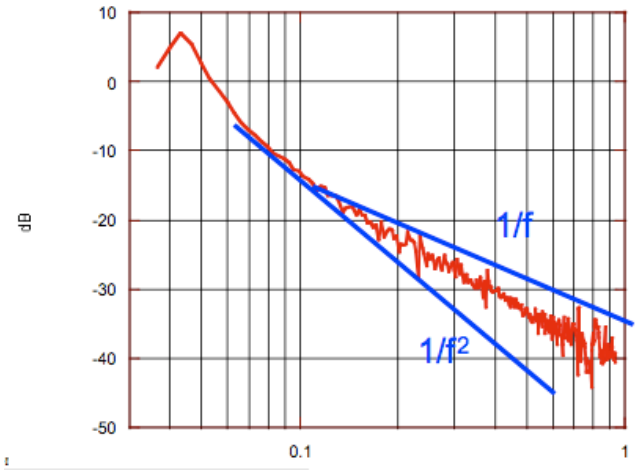

The same effect was already observed in the past low frequency measurement.

The effect is not totally understood. An explanation invoking the hysteresis of the blades has been proposed but it is still under investigation.

Chapter 6

CONCLUSIONS AND NEXT STEPS

The experiment demonstrated the possibility to compensate for the inertial limit of the GAS filter in a fully passive mechanical way. It showed that a negative center of percussion effect externally introduced by a light wand with a counterweight is able to improve the vertical attenuation of one order of magnitude. It is remarkable how such an economic solution – not just for the cost but for its simplicity too – let us to achieve a 10^{-4} attenuation factor. The effect on the transfer function of the system is so important to be measured by our rather primitive testing setup. This lets us believe that with a better excitation system, free of many of the mechanical complications which ours had, and a better measurement apparatus the performance could be even improved by a finer tuning of the counterweight.

Learning on the prototype we proposed a refined project which will be immediately implemented in the HAM SAS optic table seismic attenuators. These improved GAS filters will also be implemented in the LCGT interferometer and, likely, in other mirror suspension chains of future interferometers.

The followings are drawings of the wand as it will be mounted on the HAM SAS optical bench.

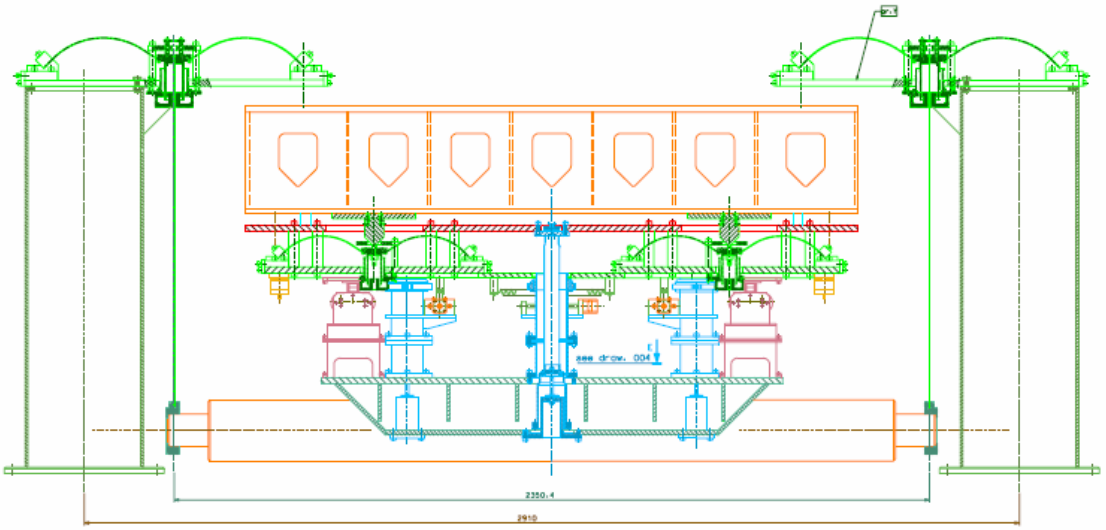

The HAM SAS with the GAS springs as suspensions

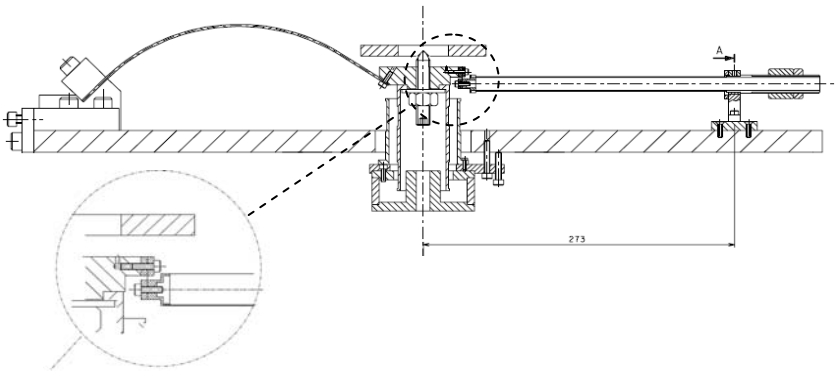

The wand will be hinged to the monolithic blades in a better way. A new counterweight sustain has been designed and dimensions are now adapted to stay into the retainer ring.

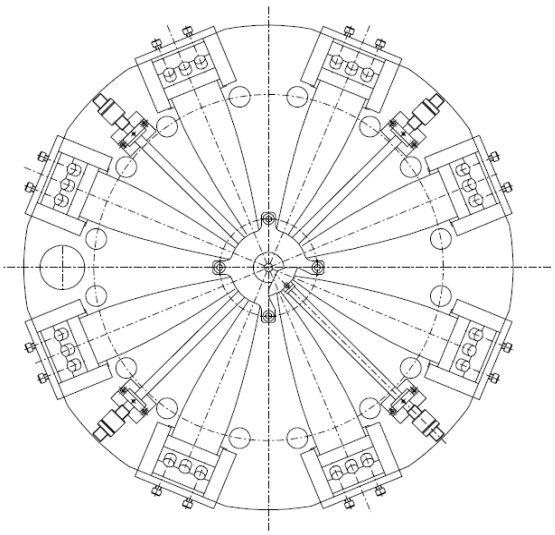

Up to 4 wands can be mounted to one filter.

Acknowledgements

I would like to thank: my supervisor Prof. Francesco Fidecaro who gave me the extraordinary opportunity to work at the California Institute of Technology. My special thanks go to my mentor and supervisor in the US Riccardo De Salvo for committing me a successful project, being always present and for all the good time spent with him in the lab. I am also indebted to: Virginio Sannibale, from Caltech, for his help and useful discussions about the experiment; John Miller, Marco Tarallo, Chiara Vanni and Juri Agresti for all their support for my work and their enjoyable company in the office; the National Science Foundation which granted for the SURF program; Caltech, California and the United States for being wonderful place to spend the summer.

Bibliography

[1]A. Bertolini, “High sensitivity accelerometers for gravity experiments” Tesi di Dottorato di Ricerca in Fisica, Università di Pisa, Classe di Scienze, XIII Ciclo, Italia

[2]A. Bertolini, G. Cella et al., Seismic Noise Filters, Vertical Resonance Frequency Reduction with Geometric Anti-Springs, a Feasibility Study” -LIGO-P990001-00-D Jan, 10 1998

[3]A. Bertolini, G. Cella et al., “SAS Vaseline Design and Prototypes Test Program Plan” LIGO-T000029-00-D

[4]A. Bertolini et al, “Report to NSF on the TAMA-SAS Passive Seismic Attenuation Chain Test for the Tokyo University 3 meter Interferometer”, LIGO- T010006-00-R

[5]H. Brody, "The sweet spot of a baseball bat," American Journal of Physics, 54(7), 640-643 (1986)

[6]R. Desalvo, H. Tariq et al.:"Study of Quality Factor and Hysteresis Associated with the State-of-the-art Passive Seismic Isolation System for Gravitational Wave Interferometric Detectors”, LIGO-P-040002-00-D

[7]M. Mantovani, R. DeSalvo, “One Hertz Seismic Attenuation for Low Frequency Gravitational Waves Interferometers”, accepted for publication on Nucl. Instr. and Meth. (2005),

[8]M. Mantovani, “Minimizing the Resonant Frequency of MGAS Springs for Seismic Attenuation System in Low Frequency Gravitational Waves Interferometers” Tesi di Laurea Specialistica 2004, LIGO-P040025-00-D

[9]G.Losurdo, et al.: “An inverted pendulum pre-isolator stage for VIRGO suspension system” Rev. Sci. Instrum., 70, 2507-2515 (1999)

[10]G.Losurdo "Ultra-Low Frequency Inverted Pendulum for the VIRGO Test Mass Suspension." Tesi di Dottorato di Ricerca in Fisica, Scuola Normale Superiore di Pisa - Classe di Scienze, Italia Ottobre 1998

[11]R. Saulson, “ Foundamentals of Intefrrometric Gravitational Waves Detector Peter” World Scientific

[12]D. Sigg, “Gravitational Waves”, Proceedings of TASI 98, LIGO-P980007-00-D

[13]A. Takamori, “Anatomy of the TAMA SAS seismic attenuation system” LIGO-P010034-00-D

[14]A. Takamori, “Low Frequency Seismic Isolation for Gravitational Wave Detectors”, PhD Thesis, LIGO-P-030049-00-R

[15]H. Tariq, et al. ”The Linear Variable Differential Transformer (LVDT) Position Sensor for Gravitational Wave Interferometer Low-frequency Controls” Nuclear Instruments and Methods in Physics Research Section A, Volume 489, Issue 1-3, p. 570-576.